J. Fluid Mech. (1979), *vol.* 93, *part* 3, *pp.* 549–584
Printed in Great Britain

The inner regions of annular jets

By N. W. M. KO AND W. T. CHAN
Department of Mechanical Engineering, University of Hong Kong, Hong Kong

(Received 8 November 1978)

Further experiments on the detailed study of annular jets are described in which the mean and fluctuating properties in the inner region have been measured. The experiments in the conical jet† have shown, besides the jet vortices in the outer mixing region, another train of vortices in the inner region. This train of vortices is due to the wake formed by the boundary layer on the surface of the conical bullet.

The experiments in the inner region of the basic annular jet have similar mean velocity profiles to those in the internal recirculating region. Good correlation is found for the location of the vortex centre, the location of reattachment, the minimum and maximum mean static pressure and their locations with the non-dimensional available pressure $M_o/A_i P_{\text{atm}}$ for entrainment behind the interface. A train of wake vortices is generated in the internal recirculating region and a train of jet vortices is found in the inner mixing region. Both types of vortices in the inner region seem to decay fairly rapidly within a distance of one outer diameter D_o downstream.

The disturbances associated with the wake vortices in the inner region seem to excite the outer mixing region. This results in another wave or train of vortices observed in the outer shear layer in addition to the jet vortices which are already in existence.

1. Introduction

The initial region of annular jets, as reported by the authors (Ko & Chan 1978), was divided into the initial merging, the intermediate and the fully merged zones. This division was based on the similarities of the mean velocity and turbulence intensity profiles in these three zones. It was further found that the similarity curves of the mean velocity and turbulence intensity profiles agreed very well with those of a single jet.

In the more recent work of the authors (Chan & Ko 1978) a simple model was proposed for the flow structure in the outer mixing region of the three annular jets considered. It was found that the outer mixing region of annular jets could be considered as the result of the shearing of a jet having a mean exit velocity $\overline{U}_o$ and a diameter D_o with the ambient liquid. D_o was the outer diameter of the annular jets. Again, as with the results of the mean velocity and turbulence intensity (Ko & Chan 1978), agreement of the structures with those of a single jet has also been found.

The above findings of the authors are mainly concerned with the flow structure within the outer mixing region of annular jets. Except for limited discussion, the

† In this paper, annular jets are called 'basic' if there is no 'bullet' in the centre of the jet; and 'conical' or 'ellipsoidal' if such a bullet (of conical or ellipsoidal shape, respectively) is present.

0022–1120/79/4258–6800 $02.00

authors did not really present details of the flow structure in the inner region of annular jets.

For the basic annular jet the inner region consisted of the inner mixing region and the internal recirculating region immediately downstream of the interface at the nozzle exit. The inner mixing region was formed by the shearing of the air emerging from the annular jet exit with the entrained air in the central axis. Owing to the absence of any supply of air in the centre, air from the main stream was entrained, resulting in the formation of the internal recirculating region and its standing vortex (Chigier & Beer 1964; Beer & Chigier 1972). The extent of this standing vortex and the maximum reverse flow rate depended on both the blockage ratio $(D_i/D_o)^2$ and the divergent angle α of the forebody (Davies & Beer 1969).

For the conical and ellipsoidal annular jet the presence of the bullet eliminated the internal recirculating region found in the basic annular jet. The inner region then consisted of the surface boundary layer and the wake which was formed behind the bullet in the intermediate zone. The wake of the conical and ellipsoidal jet was different from the case of the basic annular jet which has a uniform annular potential core surrounding an inner mixing region, since it was the result of flow which was no longer uniform.

The intention of the present investigation was to look much more closely into the flow structure in the inner region of the three annular jets considered. Besides the mean properties of the flow, such as the velocity and static pressure, the pressure fluctuations and their spectra will be presented. It is based on these measurements that the wake vortices, which are associated with the flow structure, will be isolated.

2. The model

As suggested by the simple model of Chan & Ko (1978), two mixing regions which are separated by an annular potential core, are found in the initial merging zone (figure 1). The outer mixing region has been found to be the result of the shearing of a jet having a mean exit velocity $\overline{U}_o$ and a diameter D_o with the ambient liquid. For the inner mixing region, however, the flow structures depend on the configuration of the forebody present. For the basic annular jet, the inner mixing region can be considered as the flow of a uniform stream over one end of an infinitely long cylinder, with its axis aligned parallel to the direction with the stream ($\alpha = 0$). The end face of the cylinder is made flush with the jet exit plane. Thus, the region immediately behind the forebody is occupied by a standing vortex (Carmody 1964; Chigier & Beer 1964; Davies & Beer 1969). The shedding of the standing vortex forms an array of toroidal vortices propagating downstream.

For the conical and ellipsoidal annular jet, the end of the cylinder is modified by adding the appropriate bullet. As the length of the bullet almost traverses the extent of the initial merging zone (Ko & Chan 1978), the inner mixing region can be considered as the boundary layer of a uniform flow over a surface of negative pressure gradient. The uniform flow is basically due to the uniform flow of the annular potential core. The very gradual change in the surface profiles of the bullet causes the shedding of the wake vortices very near the rear end.

In the intermediate merging zone, the disappearance of the potential core and its uniform flow implies that the wake formed is no longer submerged in a uniform

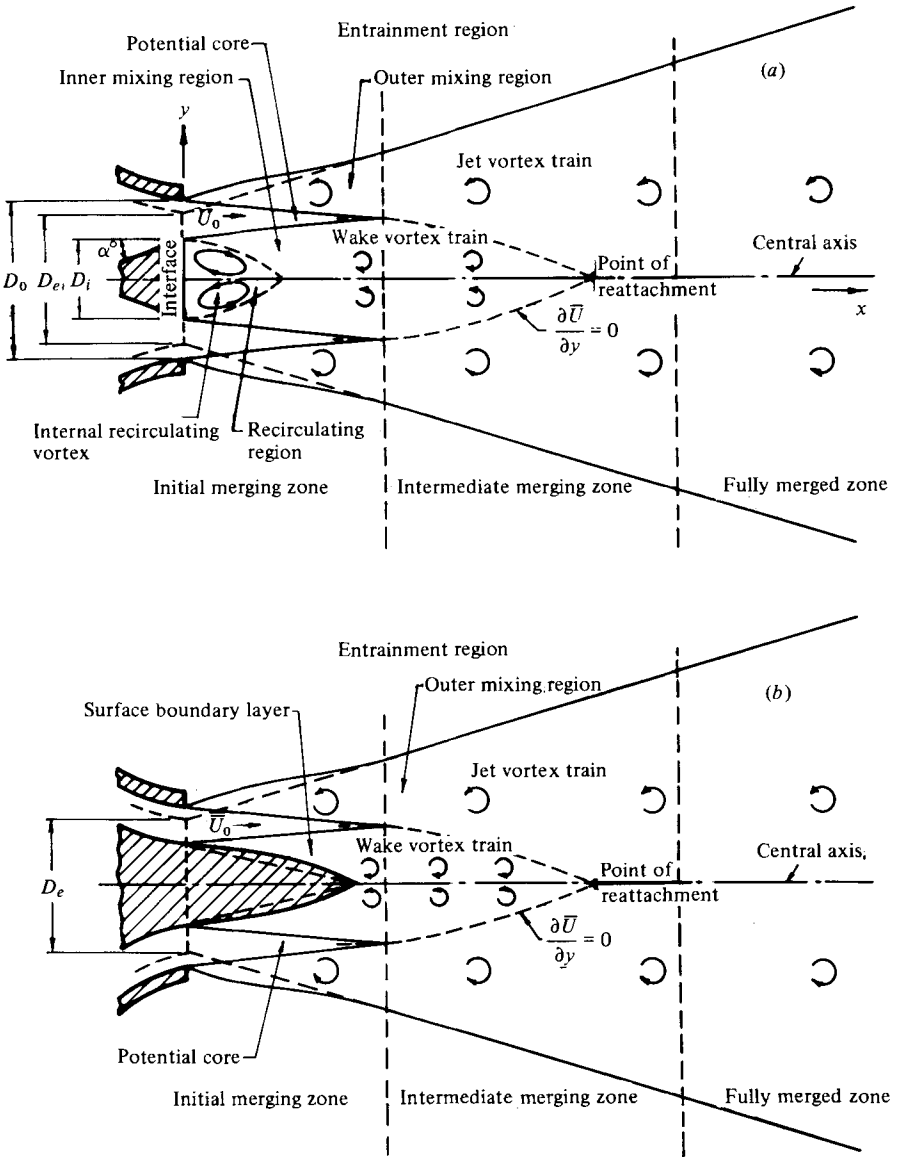

FIGURE 1. Schematic diagrams of annular jet, (*a*) without and (*b*) with bullet.

stream. This means that the surrounding stream, due to the spreading jet (Ko & Chan 1978; Chan & Ko 1978) will modify the rate of energy and mass transfer across the wake formed. This may result in more rapid degeneration of the wake and its associated vortices.

3. Apparatus

The test rig has been described in detail in Ko & Chan (1978). The outer diameter of the jet was 6·2 cm while the diameter of the interface and the base diameter of the conical and ellipsoidal bullet were 2·8 cm, giving the width of the annular slit 1·7 cm.

In all the three configurations (the basic annular, the conical and the ellipsoidal) the blockage ratio $(D_i/D_o)^2$ was 0·78 and divergent angle α of the forebody was 0°. The length of the conical and ellipsoidal bullet was 1·5 D_o, were D_o was the outer diameter.

The velocity measurements were obtained by constant temperature hot-wire anemometer. The wire used was of 5×10^{-6} m diameter tungsten wire with a sensing length of 2 mm. Inside the internal recirculating region of the basic annular jet, the response of the hot wire was spurious because any reverse flow would not be distinguished by the single hot wire used (Beer & Chigier 1972). Thus, there would be some uncertainty in the interpretation of the mean velocity measurements. However, since the maximum reverse velocity was estimated to be 0·35 $\bar{U}_o$ at the central axis and was observed to be much smaller away from the central axis, no correction was performed on the data obtained.

Besides the velocity measurements, the mean static pressure inside the inner region of the basic annular jet was also made with a disk static probe. The probe was similar (but more compact) to the probe of Miller & Comings (1957). It consisted of a 6·35 mm diameter disk having a hole of 0·36 mm diameter. The hole was connected with an internal passage to the edge of the disk and then to the manometer. The angular position of the disk pressure probe was obtained from a graduated scale having 1° divisions.

Calibration of the disk pressure probe over the velocity range considered showed that the probe was insensitive to the angle of yaw of $\phi = \pm 2°$ and was practically insensitive to the angle of pitch. It was also found that for mean velocity greater than 30 m s^{-1} the disk probe gave a pressure coefficient of 0·078. This was compared with the value for a standard disk probe of 0·115 of Bryer & Pankhurst (1971).

The pressure fluctuations were obtained by using the standard Brüel and Kjaer $\frac{1}{8}$ in. condenser microphone with the proper nose cone. The frequency spectrum of the pressure signals was obtained with the Brüel and Kjaer frequency analyser type 2107 and Brüel and Kjaer level recorder type 2307. Six per cent bandwidth filters were used for the spectral analysis.

The domain of the present investigation was mainly limited to the inner region found in the initial and in the intermediate merging zones, which extended to the axial distance of 5 D_o from the jet exit (Ko & Chan 1978). The mean jet exit velocity range varied from 10 to 50 m s^{-1}. Unless otherwise stated, the results presented were taken at a jet exit velocity of 50 m s^{-1}.

4. Mean velocity

Owing to the size of the jet, it was impractical to use the conventional yaw tube in determining the flow direction in the inner region. Therefore, the backflow in the internal recirculating region of the basic annular jet was determined intuitively from the velocity profiles obtained by hot wire. Figure 2 shows the radial distribution of the mean velocity $\bar{U}/\bar{U}_o$ of the basic annular jet within the first 0·5 D_o of the jet. Within the potential core the mean velocity ratio is basically uniform, with a ratio of about unity. However, very near the boundary of the potential core with the inner mixing region the mean velocity is slightly higher than the jet exit velocity $\bar{U}_o$, giving a ratio of slightly higher than unity. This phenomenon of the higher velocity at the inner boundary may be partly due to the profile of the forebody inside the nozzle or

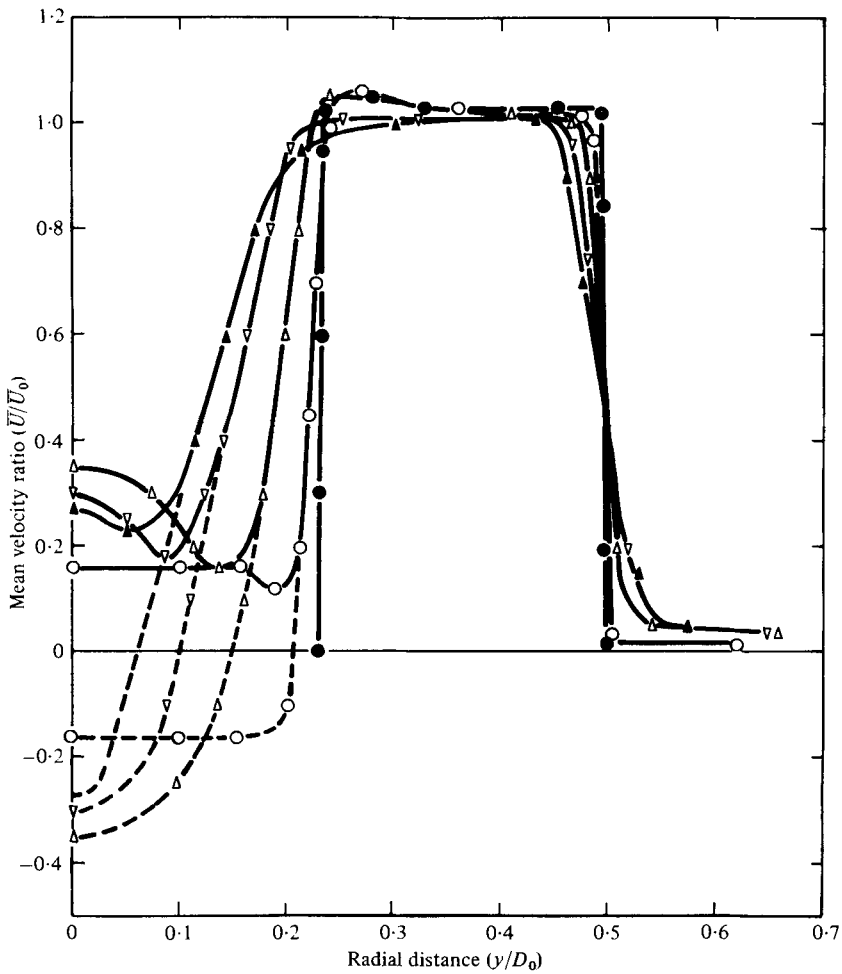

FIGURE 2. Mean velocity ratio in initial merging zone of basic annular jet. x/D_o: ●, 0; ○, 0·125; △, 0·25; ▽, 0·375; ▲, 0·438.

partly due to the entrainment of the annular jet and the resulting static pressure which is below atmospheric pressure (Miller & Comings 1960; Chigier & Beer 1964).

Beside the small peak at the inner boundary, another peak is found near and at the central axis (figure 2). The peak may be due to the limitation of a single hot wire within a flow field where instantaneous flow reversal occurs (Beer & Chigier 1972, p. 230). However, the peak is found within the first 0·5 D_o downstream of the nozzle exit, where the reverse flow exists in the internal recirculating region (Chigier & Beer 1964; Chan & Ko 1978). In this respect the mean velocity distribution around the peak is arbitrarily reversed in sign. The interpolated distribution curves are shown as dotted in figure 2.

Similarity of the mean velocity profiles in the internal recirculating region has been attempted and is shown in figure 3. The mean velocity ratio $\Delta\bar{U}/\Delta\bar{U}_m$ and the non-dimensional radial distance $\Delta y_c/\Delta y_b$ are based on the ones suggested by Abramovich

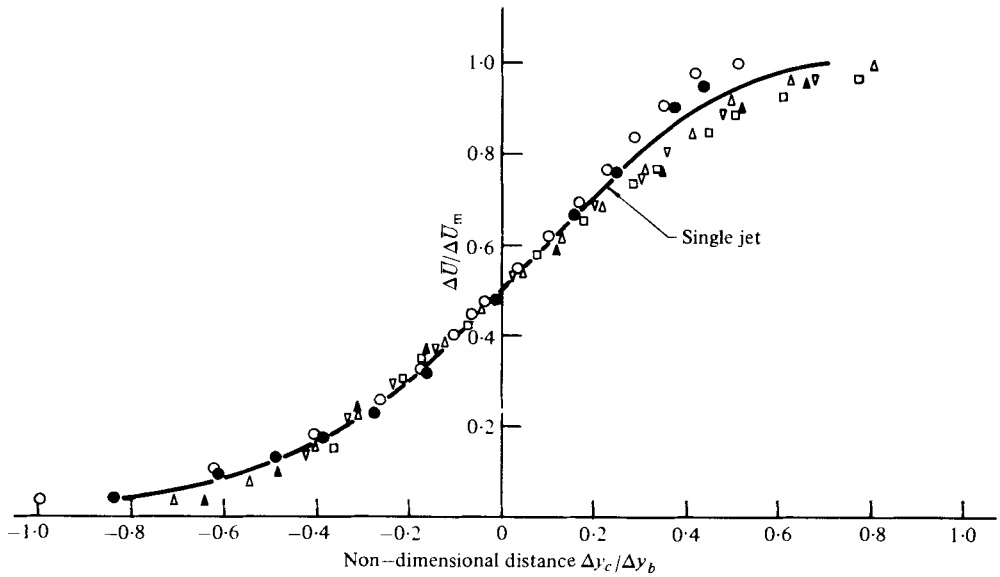

FIGURE 3. Similarity of mean velocity ratio in the inner region of basic annular jet. x/D_i: ○, 0·55; △, 0·82; ▽, 0·97; □, 1·10. (Abramovich 1963, p. 34): x/D_i: ●, 0·67; ▲, 1·10.

& Vaffin (Abramovich 1963, p. 34) of a confined axisymmetric annular jet. $\Delta\bar{U} = \bar{U} - \bar{U}_{\min}(\bar{U}_{\min} < 0)$ and $\Delta\bar{U}_m = \bar{U}_{\max} - \bar{U}_{\min}$; $\Delta y_c = y - y_{0\cdot5}$ and

$$\Delta y_b = y_{0\cdot9} - y_{0\cdot1} \cdot y_{0\cdot9},$$

and $y_{0\cdot1}$ are the radial positions where the local mean velocity is equal to 0·9, 0·5 and 0·1 of $\bar{U}_m$. Good agreement is found for the mean velocity profiles. The confined annular jet results of Abramovich & Vaffin agree with those of the present investigation. In addition, the results of the single jet are found to be similar to those of the annular jet.

No agreement of the mean velocity deficit is observed for the inner region downstream of the standing vortex. It is conceivable that such agreement in a turbulent wake does not occur till far downstream of the obstacle (Carmody 1964).

The corrected and interpolated velocity distribution curves were used to calculate the streamline pattern of the recirculating region. As the flow direction was not really known, successive iterations of the streamlines were necessary. It was first assumed that the measured velocity was the axial component. From the assumption a coarse streamline chart was constructed. The flow direction was estimated from the chart for further iterations.

The streamline chart within the first 1·5 D_o of the basic annular jet is shown in figure 4. The unit of the stream function is ψ/ψ_o, where $\psi_o = 4/\{\bar{U}_o(D_o^2 - D_i^2)\}$. As in the case of Chigier & Beer (1964) and Davies & Beer (1969), the internal recirculating region is found immediately behind the interface of the basic annular jet and is indicated by the streamline of zero. This recirculating region is mainly found within the first 0·5 D_o downstream of the interface and is within the radial position of the inner diameter D_i. The maximum back flow rate is about 2·5 % of the output flux at the nozzle exit and it occurs roughly at the axial plane $x/D_o = 0{\cdot}25$.

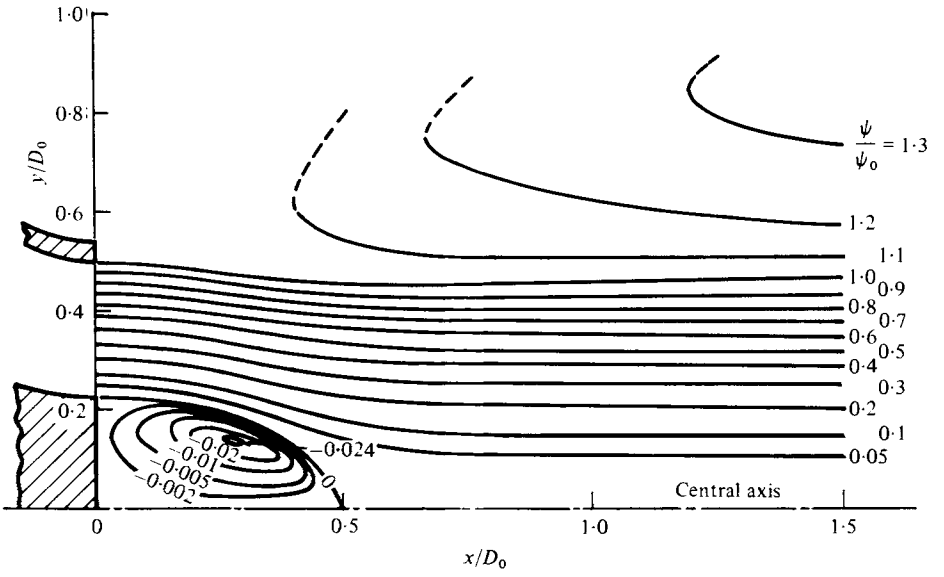

FIGURE 4. Streamlines of flow in basic annular jet.

Even though the streamline chart of figure 4 is similar to the one of Chigier & Beer (1964), however, differences are found between them. The most obvious difference is the location of the vortex centre of the stationary vortex found in the internal recirculating region. This difference is expected because of the differences in the geometrical conditions of the nozzle and the interface and in the flow condition at the nozzle exit.

Attempts at correlating the position of the vortex centre of annular jets having a different configuration and flow condition have been made and are shown in figure 5. Unfortunately, the available results from other workers are very limited. In figure 5 the axial and radial positions of the vortex centre are correlated with the non-dimensional parameter of $M_o/A_i P_{\text{atm}}$, where M_o is the momentum flux at the nozzle exit, A_i the area of the interface and P_{atm} the atmospheric pressure. Besides the results of the present nozzle configuration, results of the two-dimensional duel jets of Miller & Comings (1960) and of the twin coaxial annular hot and cold air jets of Barrett & Tipping (1962) are also included. For the latter results of Barrett & Tipping (1962), the estimate of the location was based on the assumption that the outer cold coaxial jet did not affect the location of the vortex centre of the inner hot annular jet.

Good correlation of the axial and radial positions of the vortex centre is found with the non-dimensional parameter $M_o/A_i P_{\text{atm}}$ (figure 5). This non-dimensional parameter really represents the pressure available for the entrainment behind the interface. It is interesting to find that the radial position y_c/D_o of the vortex centre is more or less independent of the non-dimensional pressure $M_o/A_i P_{\text{atm}}$ and has a value roughly equal to 0·18. The axial position x_c/D_o, however, is found to decrease with the increase in the $M_o/A_i P_{\text{atm}}$. In other words, at higher available pressure, the vortex centre is shifted more towards the nozzle exit. This phenomenon seems physically logical because with the higher momentum flux available at the nozzle exit, say, higher entrainment would occur in the region behind the interface. This would result in the

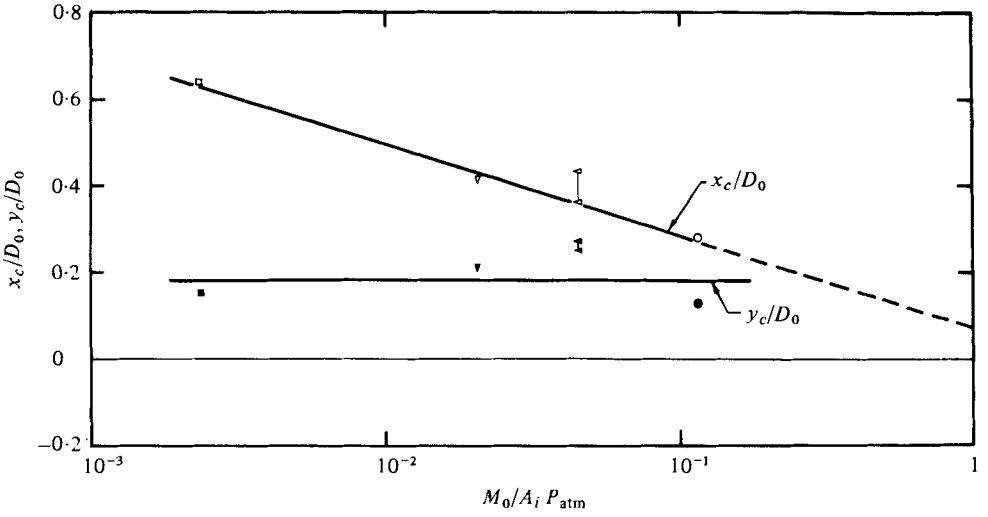

FIGURE 5. Location of vortex centre. ○, 50 m s^{-1}; □, Miller & Comings (1957); ▽, Chigier & Beer (1964); ◁, Barrett & Tipping (1962).

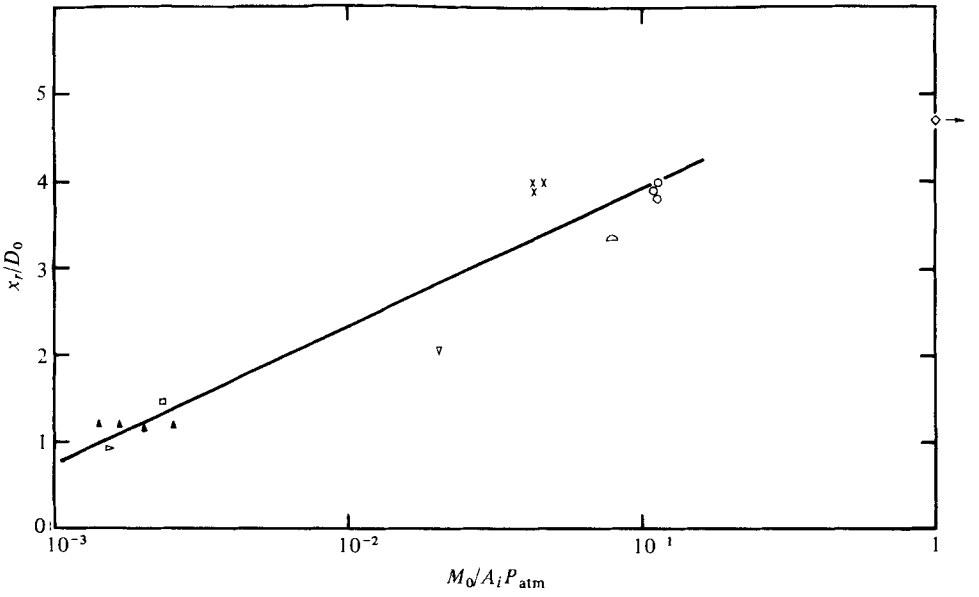

FIGURE 6. Variation of reattachment position with non-dimensional available pressure. ×, 30 m s^{-1}; ⌓, 50 m s^{-1}; ▷, Ayukawa & Shakouchi (1976); ▲, Tanaka & Tanaka (1978); ◇, single jet. Other symbols same as in figure 5.

shifting of the vortex more towards the interface. Correspondingly, similar phenomenon would be observed if the area of the interface A_i were reduced. Extrapolation of the results suggests that the vortex centre appears at the interface when the available pressure $M_o/A_i P_{atm}$ equals to 2·2.

Based on this non-dimensional pressure, the results of the position of reattachment of annular jets (Ko & Chan 1978) are re-correlated (figure 6). Besides the results of the present study, results of Miller & Comings (1960), Chigier & Beer (1964), Ayukawa & Shakouchi (1976) and Tanaka & Tanaka (1978) are shown. The combined

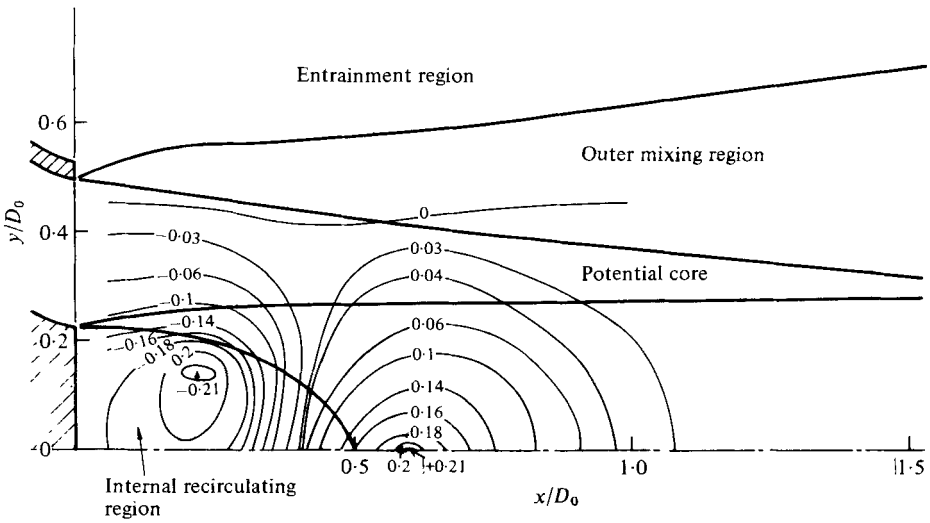

FIGURE 7. Mean static pressure contours of basic annular jet. (The numbers labelling the curves are $\bar{p}_s/(\frac{1}{2}\rho_o\bar{U}_o^2)$ expressed as a percentage.)

single jet results of Laurence (1956), Davies, Fisher & Barratt (1963) and Ko & Davies (1971), which has an infinite available pressure, are also included in the figure. Though the correlation is not as good as the one using the diameter ratio D_o/D_i, the fairly good agreement further supports the validity of the available pressure to describe the conditions behind the interface. Again, the higher the available pressure, say, the higher the momentum flux at the nozzle exit, and the larger the axial distance where reattachment occurs. Nevertheless, the position would approach the limiting position of single jet, which is about 0·47 D_o downstream of the nozzle exit.

5. Mean static pressure

The mean static pressure distribution $\bar{p}_s/\frac{1}{2}\rho_o\bar{U}_o^2$ inside the basic annular jet is shown in figure 7. Basically, it is similar to the result of Chigier & Beer (1964) that subatmospheric static pressure is found within the internal recirculating region and is followed by the region of static pressure above atmospheric. It is within this above-atmospheric region that the stagnation point is located.

The subatmospheric region behind the interface covers not only the area immediately behind the interface up to $x/D_o \simeq 0{\cdot}4$, but also extends into the potential core (figure 7). The iso-contour of the atmospheric pressure $\bar{p}_s/\frac{1}{2}\rho_o\bar{U}_o^2 = 0$ is found to be extended nearly to the outer mixing region. The minimum mean static pressure is found within the internal recirculating region and is equal to $-0{\cdot}21$ of the velocity head at the nozzle exit. The position of the minimum pressure is located at $x_m/D_o = 0{\cdot}22$ and $y_m/D_o = 0{\cdot}14$.

The above-atmospheric region starts from the axial position $x/D_o \simeq 0{\cdot}4$ up to about 1·2. It also extends into the potential core of the jet. The stagnation pressure has a value of 0·21 of the velocity head at the nozzle exit. The value, irrespective of the sign, is the same as the one of the minimum static pressure. Its position is found at $x/D_o = 0{\cdot}6$ and the central axis $y/D_o = 0$.

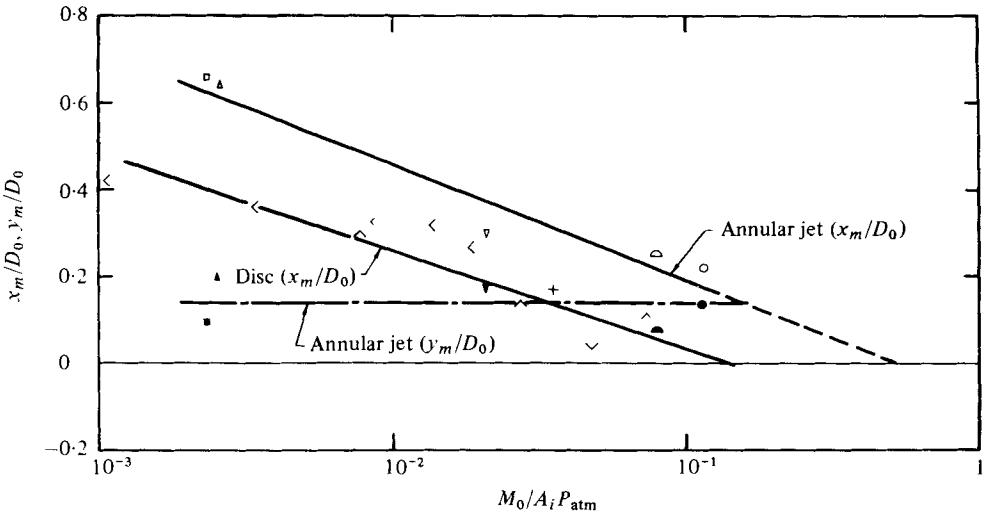

FIGURE 8. Location of minimum mean static pressure. Basic annular jet: ○, 50 m s^{-1}; ⌓, 30 m s^{-1}; □, Miller & Comings (1957); △, Tanaka & Tanaka (1978). Disk: +, Carmody (1964); ∧, Davies & Beer (1969); ∨, Sullerey *et al.* (1975); <, Durão & Whitelaw (1978).

The location of the minimum mean static pressure has also been correlated with the non-dimensional pressure M_o/A_iP_{atm} (figure 8). Again, the available annular-jet results from other workers are also very scanty. However, the same trend of nearly constant y_m/D_o and decreasing x_m/D_o with the increase in M_o/A_iP_{atm}, as the ones of the vortex centre (figure 5), is also found. Nevertheless, the location of the minimum pressure is slightly more towards the central axis and more towards the interface than the one of the vortex centre. Extrapolation of the x_m/D_o results gives a zero displacement of the minimum pressure at M_o/A_iP_{atm} equal to 0·5 which is lower than the one of vortex centre of 2·2.

The available results for the axial location of the minimum mean static pressure behind a disk are also shown in figure 8. The results of Carmody (1964), Davies & Beer (1969) and Sullerey, Gupta & Moorthy (1975) are included. It is interesting to find that the axial location of the minimum static pressure behind a disk has the same trend as the one of annular jet. In addition they correlate well with the non-dimensional pressure M_o/A_iP_{atm}. It is further found that for the same value of the available pressure the location of the disk is shifted more towards the interface of the disk face rather than that of the annular jet. This is mainly due to the absence of the forebody upstream of the disk, resulting in the change of the flow characteristics before and after passing the disk.

The recent work of Durão & Whitelaw (1978) reported the mean velocity measurements in the near wake of a disk. Along the central axis behind the disk, a minimum mean velocity was found. The position of the minimum velocity varied with both the mean velocity at the nozzle exit and the diameter of the disk. Since it has been found by Miller & Comings (1960), Chigier & Beer (1964) and Davies & Beer (1969) that the axial position of the minimum mean velocity along the central axis only differed very slightly from the axial position of the minimum static pressure, the velocity results of Durão & Whitelaw (1978) are also included in figure 8. The velocity results

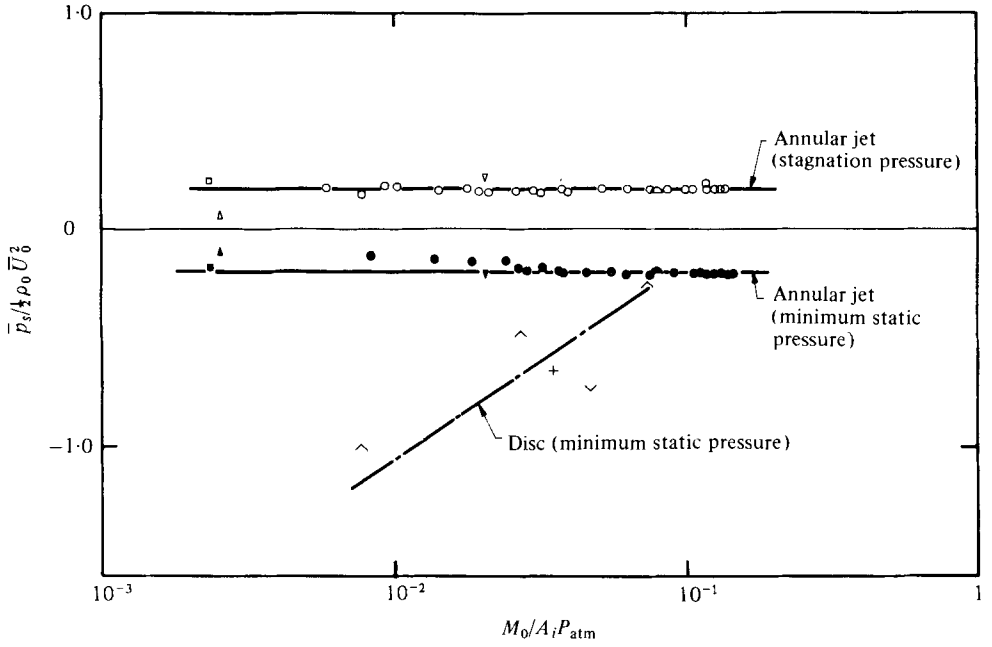

FIGURE 9. Variation of minimum mean static pressure and stagnation pressure with non-dimensional available pressure. Symbols as in figure 8.

of Durão & Whitelaw (1978) fit in very well with the correlation of the static pressure.

The correlation of the minimum static pressure and the stagnation or maximum pressure, $\bar{p}_s/\frac{1}{2}\rho_o \bar{U}_o$, of annular jet is shown in figure 9. Because the effort involved in locating the minimum and maximum static pressure was very time consuming, most of the results shown in figure 9 were obtained with the static pressure probe located at the minimum and stagnation point when the available pressure $M_o/A_i P_{atm}$ equals to 0·116. This procedure is justified since the results thus obtained are constant for the maximum static pressure and are nearly constant for the minimum static pressure. Furthermore, the results for annular jets of Miller & Comings (1960) and Chigier & Beer (1964) agree very well with those of the present investigation.

The constancy of the static pressure with the available pressure $M_o/A_i P_{atm}$ gives a value of $-0{\cdot}20$ and $+0{\cdot}18$ of the velocity head for the minimum and maximum static pressure respectively (figure 9). This means that the two static pressures are very nearly numerically equal and are about 20 % of the velocity head at the nozzle exit. This constancy of the static pressures suggests that any increase in the available pressure $M_o/A_i P_{atm}$ does not result in any increase in the ratio of the partial vacuum inside the internal recirculating region and of the stagnation pressure in the region further downstream of the recirculating region.

It has been discussed by Miller & Comings (1957, 1960) that the total momentum flux across any section of the jet is made up of the momentum flux due to the mean velocity, to the fluctuating velocity and to the static pressure. Thus, the absence of variation of the minimum and stagnation pressure with the available pressure $M_o/A_i P_{atm}$, as observed above, suggests that any increase in the available pressure

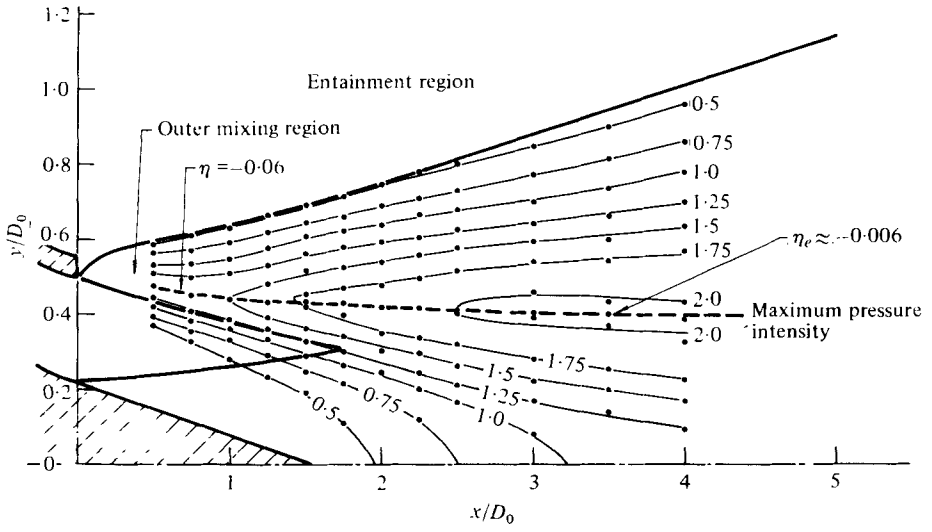

FIGURE 10. Overall pressure intensity contours of conical jet. (The numbers labelling the curves are $\tilde{p}/(\rho_o \bar{U}_o^2)$ expressed as a percentage.)

for the entrainment, owing to the increase in the nozzle exit momentum flux, does not alter the proportion of contribution of the static pressure. Rather, it is partly or wholly adjusted between the terms of mean velocity and fluctuating velocity.

The available minimum static pressures of the disk from different workers (Carmody 1964; Davies & Beer 1969; Sullerey *et al.* 1975) are also shown in figure 9. They further support the use of the available pressure defined above. The results imply an increase in the minimum static pressure with the increase in the available pressure. This indicates that any increase in the available pressure would involve the readjustment of the proportion of the contribution of mean velocity, fluctuating velocity and static pressure. The disk result achieves the same static pressure as the one of the annular jet when $M_o/A_i P_{\text{atm}}$ equals to 9×10^{-2}.

6. Overall pressure intensity

The distribution of the overall pressure fluctuations, as obtained by the microphone, within the conical jet and the basic annular jet are shown in figures 10–12. The pressure fluctuations are presented as the pressure intensity (r.m.s.) $\tilde{p}/\rho_o \bar{U}_o^2$. As far as the conical jet is concerned, the distribution of the overall pressure intensity (figure 10) is basically the same as for the ellipsoidal jet (Chan & Ko 1978). A peak is found in the outer mixing region. The locations of the maximum pressure intensity lie along $\eta = (y - D_o/2)/x = -0{\cdot}06$ for $x/D_o \leqslant 1{\cdot}25$, that is, within the initial merging zone. For $x/D_o > 1{\cdot}25$ the locations lie more parallel to the central axis,

$$\eta_e = (y - D_e/2)/x \approx -0{\cdot}006.$$

Although the results of the conical and ellipsoidal jet are basically the same, differences are found. The peak overall intensity of the conical jet is about 2·0% while that of the ellipsoidal jet 2·2%. The distribution of the overall pressure intensity of the conical jet does not indicate clearly the contribution from the wake of the bullet.

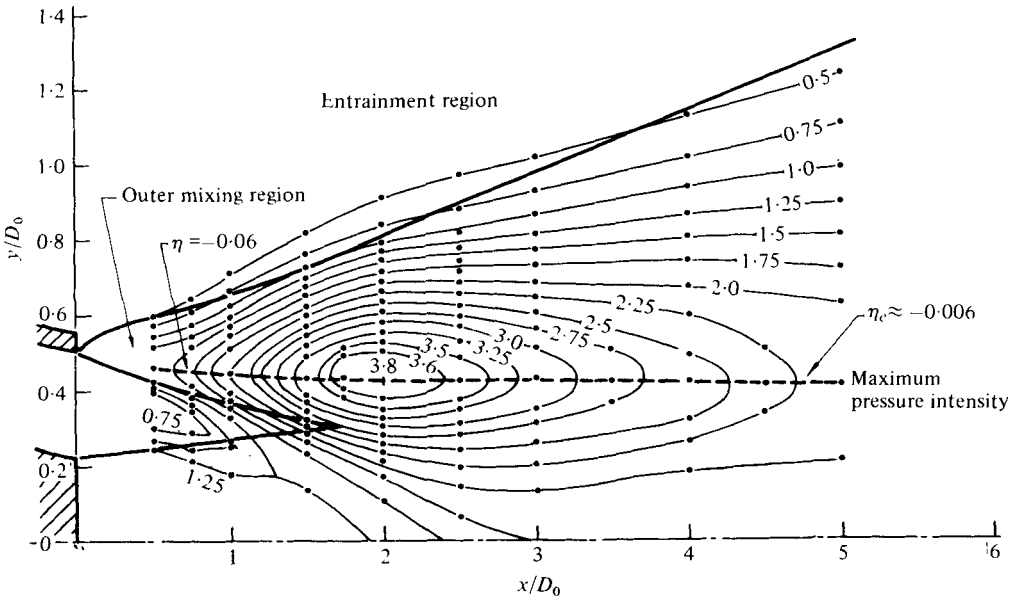

FIGURE 11. Overall pressure intensity contours of basic annular jet.

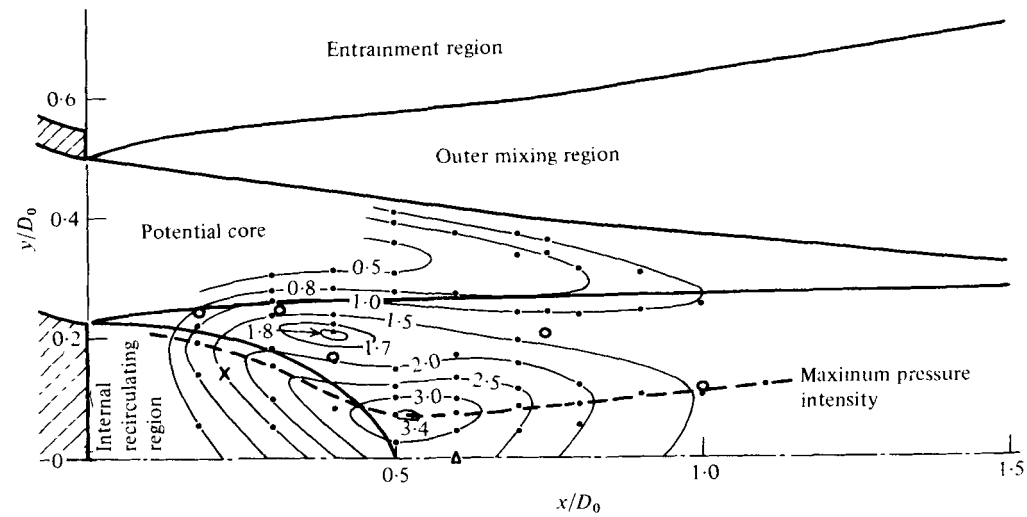

FIGURE 12. Overall pressure intensity contours within the inner region of basic annular jet. ×, minimum mean static pressure; △, maximum mean static pressure; ○, maximum pressure intensity of inner jet vortices.

As will be shown later, it is mainly because of the small contribution of the wake to the overall pressure fluctuations.

The overall pressure intensity distribution of the basic annular jet is shown in figures 11 and 12. Figure 12 shows the more detailed distribution in the inner region, that is, the internal recirculating region and the inner mixing region. Also shown in figure 12 are the locations of the maximum and minimum mean static pressure discussed above (figure 7). In the region behind the interface the contours of the overall

pressure intensity show the effect of the standing vortex and its propagation downstream. Within the recirculating region the intensity starts to build up from $x/D_0 \approx 0{\cdot}125$ and reaches a maximum at $x/D_0 \approx 0{\cdot}5$. At the axial position of $x/D_0 = 1{\cdot}0$ the intensity becomes more or less insignificant.

The locations of the maximum overall pressure intensity are also shown in figure 12. The locus lies just inside the boundary of the internal recirculating region and follows roughly the contour of the boundary. In other words, the maximum pressure intensity tends to shift towards the central axis. At the axial position of $x/D_0 = 0{\cdot}52$ the locus changes in direction and shifts gradually towards the potential core. The location of the change of direction coincides with the one of the peak pressure intensity.

The peak overall pressure intensity of the standing or wake vortices is found at $x/D_0 = 0{\cdot}52$ and $y/D_0 = 0{\cdot}08$ and has a level of 3·4 %. This is only slightly lower than the peak level in the outer mixing region of 3·8 % (figure 11). The location of the peak overall pressure intensity is different from the location of the maximum mean static pressure, and is slightly upstream and more towards the potential core. The reason for this difference is not known. It may be due to the interaction of the wake vortices on other sides of the central axis.

It has been suggested by Kwan & Ko (1976, 1977) and Chan & Ko (1978) that the locations of the maximum pressure intensity indicate the possible location of the vortices and their path of propagation downstream. Thus, the locus on figure 12 suggests that because of the entrainment in the internal recirculating region, the shedded standing or wake vortices are drawn towards the central axis. By comparing with the mean static pressure distribution of figure 7, it is found that the deflexion of the wake vortices towards the central axis is observed mainly in the region where the pressure is sub-atmospheric. The deflexion away from the central axis occurs just before the location of the maximum mean static pressure. This also indicates the loss of the effect of entrainment in the recirculating region. Further, the deflexion towards the potential core may also suggest the gradual dominance of the high momentum within the potential core. The latter can be easily seen from the path of propagation of the jet vortices in the outer mixing region (figures 10 and 11), in single jet (Ko & Davies 1975), in the coaxial jets (Kwan & Ko 1976, 1977), along $\eta_e = -0{\cdot}06$.

The overall pressure intensity contours in figure 12 also show a peak at $x/D_0 \simeq 0{\cdot}4$ and $y/D_0 \simeq 0{\cdot}2$. In addition, there is another peak along the inner boundary of the potential core with the inner mixing region. Because of the complicated interaction of the contribution from different types of vortices in the basic annular jet, the peak at $x/D_0 \simeq 0{\cdot}4$ and $y/D_0 \simeq 0{\cdot}2$ and the one along the potential core boundary may be due to the same type of vortices. These vortices, as will be discussed in more detail later, may be due to the jet vortices generated by the shearing of the flow between the potential core and the internal recirculating region.

7. Pressure spectrum

7.1. *Conical jet*

The overall pressure intensity distribution of the conical jet does not indicate clearly the contribution of the wake vortices of the bullet. However, the contribution of the wake vortices can be better illustrated by the pressure spectra obtained at the central axis (figure 13). In the spectrum the dominant peak at the low frequency regime of

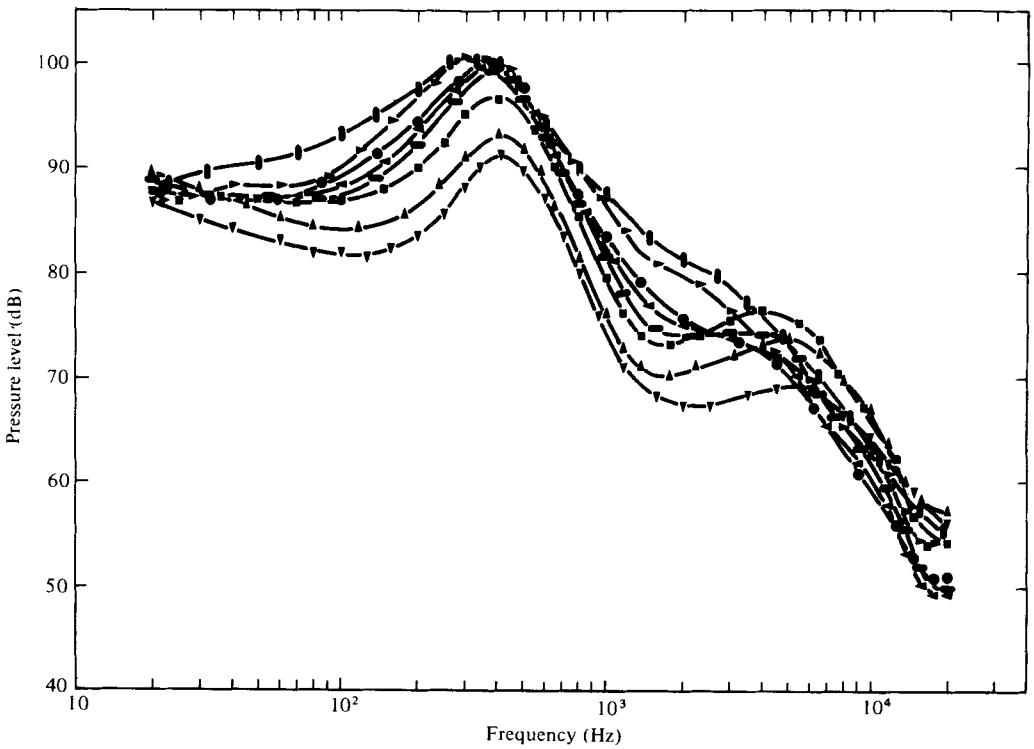

FIGURE 13. Spectra of pressure fluctuations along the central axis of conical jet ($y/D_o = 0$). x/D_o: ▼, 1·75; ▲, 2; ■, 2·5; ⬬, 3; ◀, 3·25; ●, 3·5; ▶, 4; ▮, 4·5.

300–400 Hz is due to the jet vortices generated in the outer mixing region (Chan & Ko 1978). The spectral intensity at the central axis is found to build up from $x/D_o = 1{\cdot}75$ till 4·5.

Besides the peak due to the jet vortices there is a broad peak in the high frequency regime. It is found in the axial range considered, $1{\cdot}75 \leqslant x/D_o \leqslant 4{\cdot}5$. At $x/D_o \geqslant 4$ it becomes not so obvious. The peak frequency tends to be found from 3 to 5 kHz. Also indicated by figure 13 is the distribution of the peak pressure level, which increases fairly rapidly from $x/D_o = 1{\cdot}75$ to a maximum at $x/D_o = 2{\cdot}5$, and is then masked by the level of the jet vortices at $x/D_o = 4$.

The radial distribution of the pressure spectra near the maximum peak level, $x/D_o = 2$, of the high frequency peak is shown in figure 14. The peak level decreases fairly rapidly from the central axis to $y/D_o = 0{\cdot}1$ and is nearly masked by the jet vortices at $y/D_o = 2$.

The extent of this high frequency peak can be easily seen from the contours of the pressure intensity $\tilde{p}/\rho_o \overline{U}_o^2$ because of the peak (figure 15). The pressure intensity shown in the figure was obtained from the estimation of the power under the high frequency peak in the spectrum. The highest pressure intensity is only 0·2%. It is found to start from $x/D_o = 1{\cdot}5$ and $y/D_o = 0{\cdot}1$ and deflects inwards towards the central axis. At $x/D_o = 2{\cdot}5$ it touches the central axis before it deflects away from it.

The contours in figure 15 suggest the presence of the wake vortices generated by the boundary layer on the surface of the conical bullet and their propagation downstream.

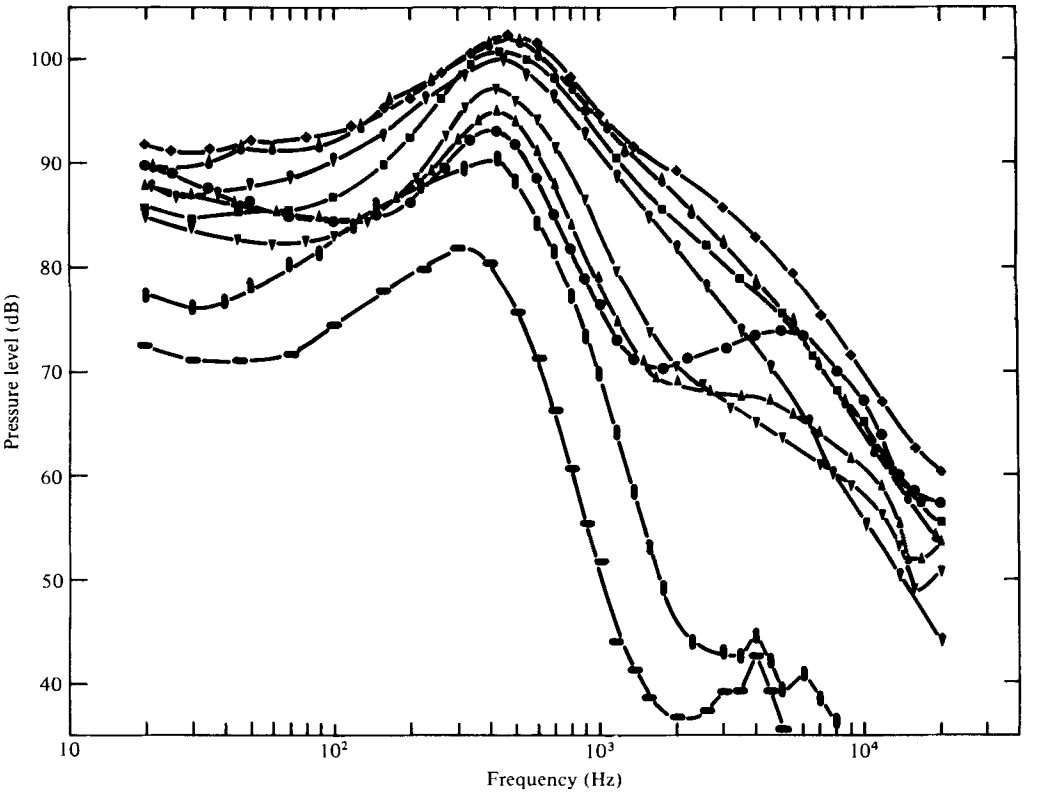

FIGURE 14. Spectra of pressure fluctuations at different radial positions of conical jet ($x/D_o = 2$). y/D_o: ●, 0; ▲, 0·1; ▼, 0·2; ■, 0·3; ◆, 0·4; ◭, 0·5; ◮, 0·6; ▮, 0·8; ⬬, 1.

These shedding wake vortices exhibit a frequency of 3–5 kHz and are due to the separation of the boundary layer from the surface. The pressure intensity of these wake vortices is small, with a maximum of 0·20 %, which is much smaller than that for the jet vortices, about 2 %. In addition, the movement of these vortices, after their shedding, tends to follow the contour of the conical bullet till the central axis.

The reason for the deflexion of the wake vortices away from the central axis is not really known. It may be due to the interaction of the wake vortices from different parts of the surface of the conical bullet. It may also represent the actual movement of the vortices before their disappearance or masked by the jet vortices further downstream.

The Strouhal numbers $St_i = f_w D_i/\overline{U}_o$ of the peak frequency of the wake vortices are shown in figure 16. The Strouhal numbers of both the conical and ellipsoidal jet are shown. As would be expected, because of the difference in the contour of the two types of bullet used, the Strouhal numbers of the two annular jets are different. The Strouhal number of the conical jet is higher than that of the ellipsoidal jet; this difference is reduced at a distance further downstream. At $x/D_o = 3$ the Strouhal numbers are the same for both jets.

The value of the Strouhal number is high. Immediately downstream of the bullet, the Strouhal number of the conical jet is 2·8 and of the ellipsoidal jet 2·2. Even at

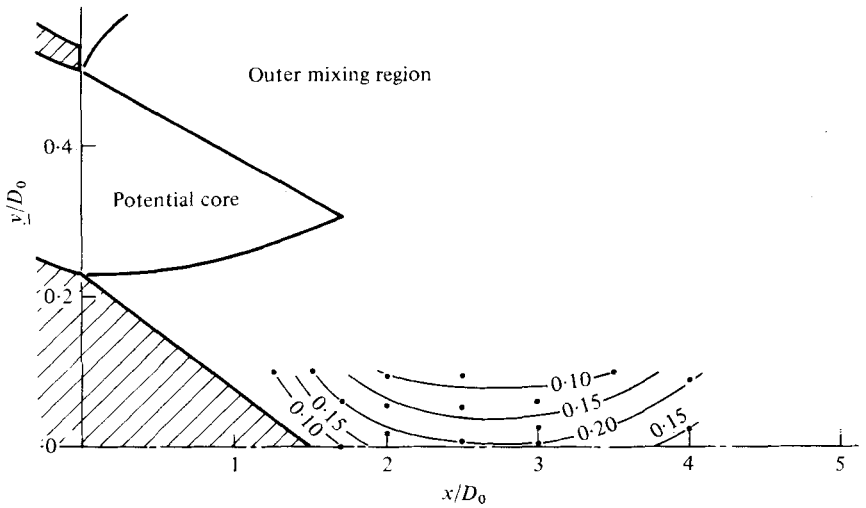

FIGURE 15. Pressure intensity contours caused by wake vortices within conical jet.

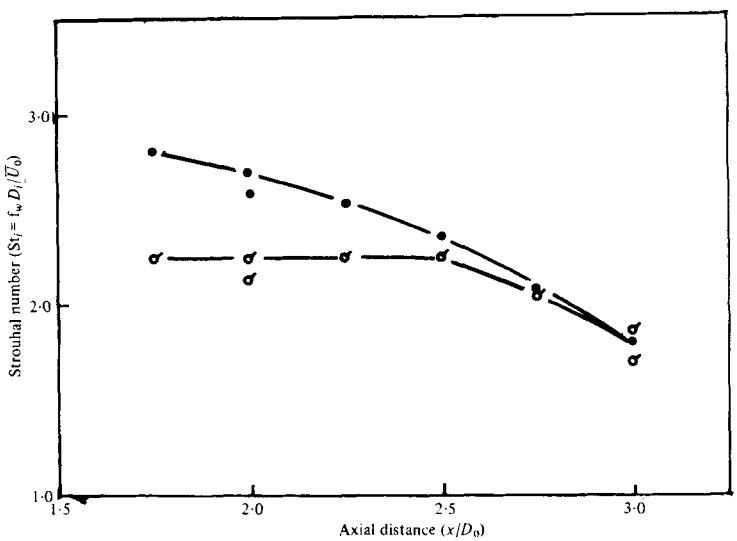

FIGURE 16. Strouhal number of wake vortices (y/D_o = 0). ●, Conical; ♂, ellipsoidal.

$x/D_o = 3$ the Strouhal number is 1·8 for both annular jets. Thus, the Strouhal number of the wake vortices of the two annular jets is much higher than that of the jet vortices, $0{\cdot}4 \leqslant St \leqslant 1{\cdot}4$.

It has been observed by Crow & Champagne (1971), Chan (1974), Bechert & Pfizenmaier (1977) and Moore (1977) that a jet would be excited at the most preferred mode. The most amplified mode is at a Strouhal number of 0·5 for the shear layer and 0·35 for the centre-line. Kwan & Ko (1976) have also observed that for any train of vortices rapid decay of the vortices would occur if their Strouhal number was different from the Strouhal number of the most preferred mode. By contrast, for a train of vortices having a Strouhal number near to that of the most preferred mode, the vortices would maintain their growth downstream. In this respect, the very high

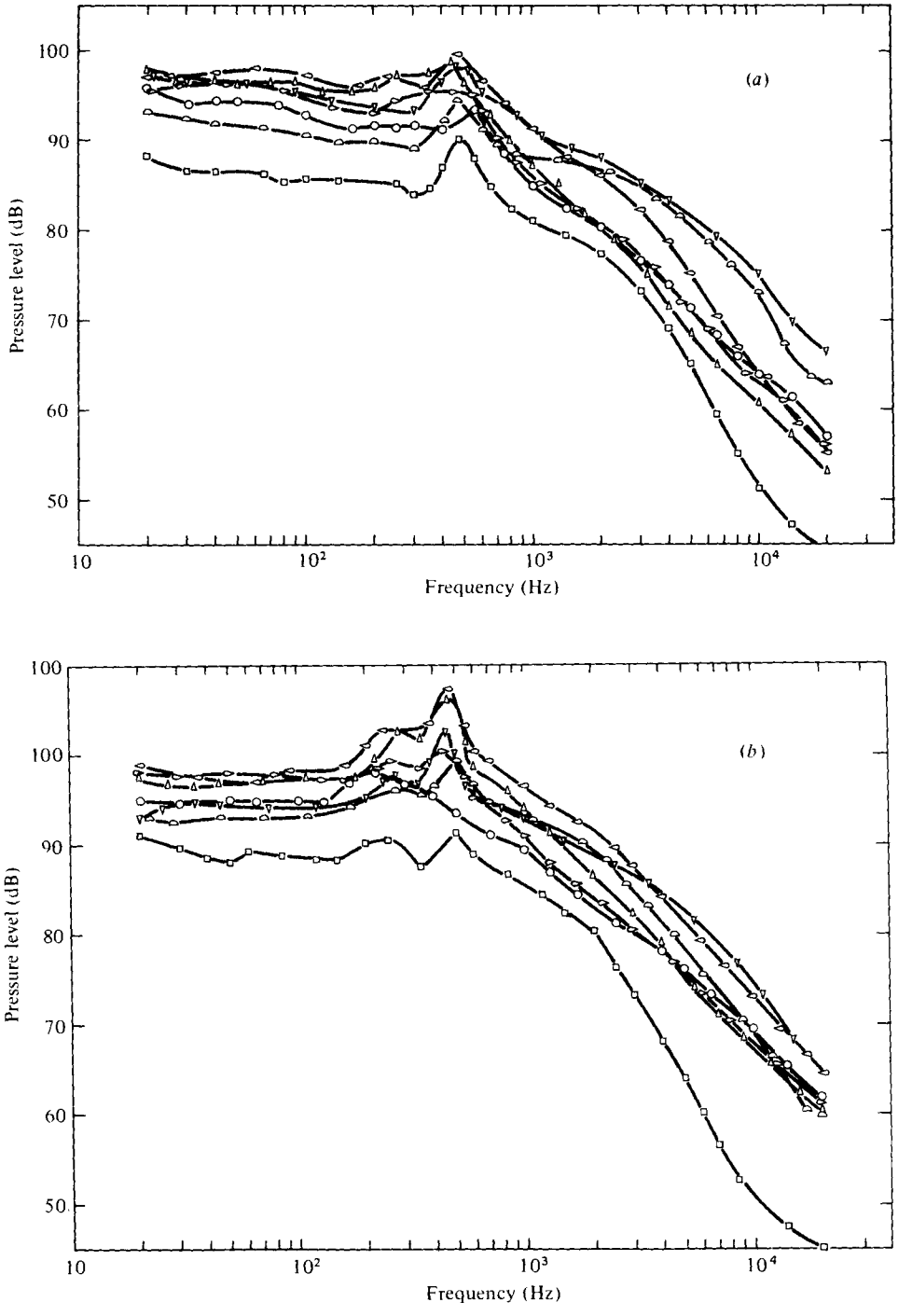

FIGURE 17. For legend see facing page.

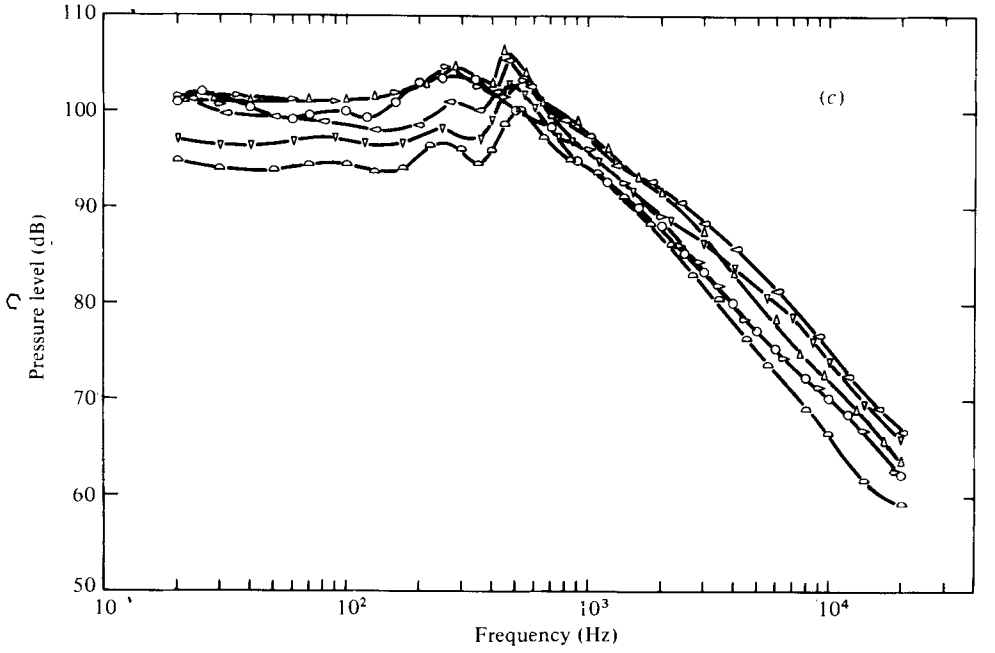

FIGURE 17. Spectra of pressure fluctuations within internal recirculating region of basic annular jet: (*a*) $x/D_o = 0{\cdot}2$; (*b*) $x/D_o = 0{\cdot}3$; (*c*) $x/D_o = 0{\cdot}4$. y/D_o: ○, 0; ⊂, 0·05; △, 0·1; ⊂, 0·15; ▽, 0·2; ⌓, 0·25; □, 0·3.

Strouhal number of the wake vortices suggests that they are not preferred and would experience rapid deterioration and disappear.

7.2. *Basic annular jet*

As has been shown above, the spectra of the conical and ellipsoidal jet are basically simple in their nature. Except in the region just behind the bullet where the wake vortices are present, the spectra in these two types of annular jet are dominated by the jet vortices generated in the outer mixing region. In the basic annular jet, however, the train of jet vortices in the outer mixing region is not the only dominant one. The presence of the strong standing vortices behind the interface and their shedding downstream would complicate the spectrum obtained. In addition, jet vortices may be generated in the inner shear layer or the inner mixing region and would complicate the matter further. The following sections will attempt to isolate the contributions from these different individual trains of vortices or waves. Since the contribution from the jet vortices generated in the outer mixing region to the spectrum has been discussed by Chan & Ko (1978), the main effort will concentrate on the contributions from the wake vortices and the inner jet vortices.

The pressure spectra within the internal recirculating region of the basic annular jet are shown in figures 17(*a*)–(*c*). In the figures two distinct peaks are found. The peak at the frequency of 460 Hz is more distinct than the other at the frequency of 230–260 Hz. Also shown in the figures the peak level of the former is always higher than the level of the latter.

The peak level of the more distinct one at 460 Hz varies with both the axial and radial position. At $x/D_o = 0{\cdot}2$ the peak level is found to have a maximum at the

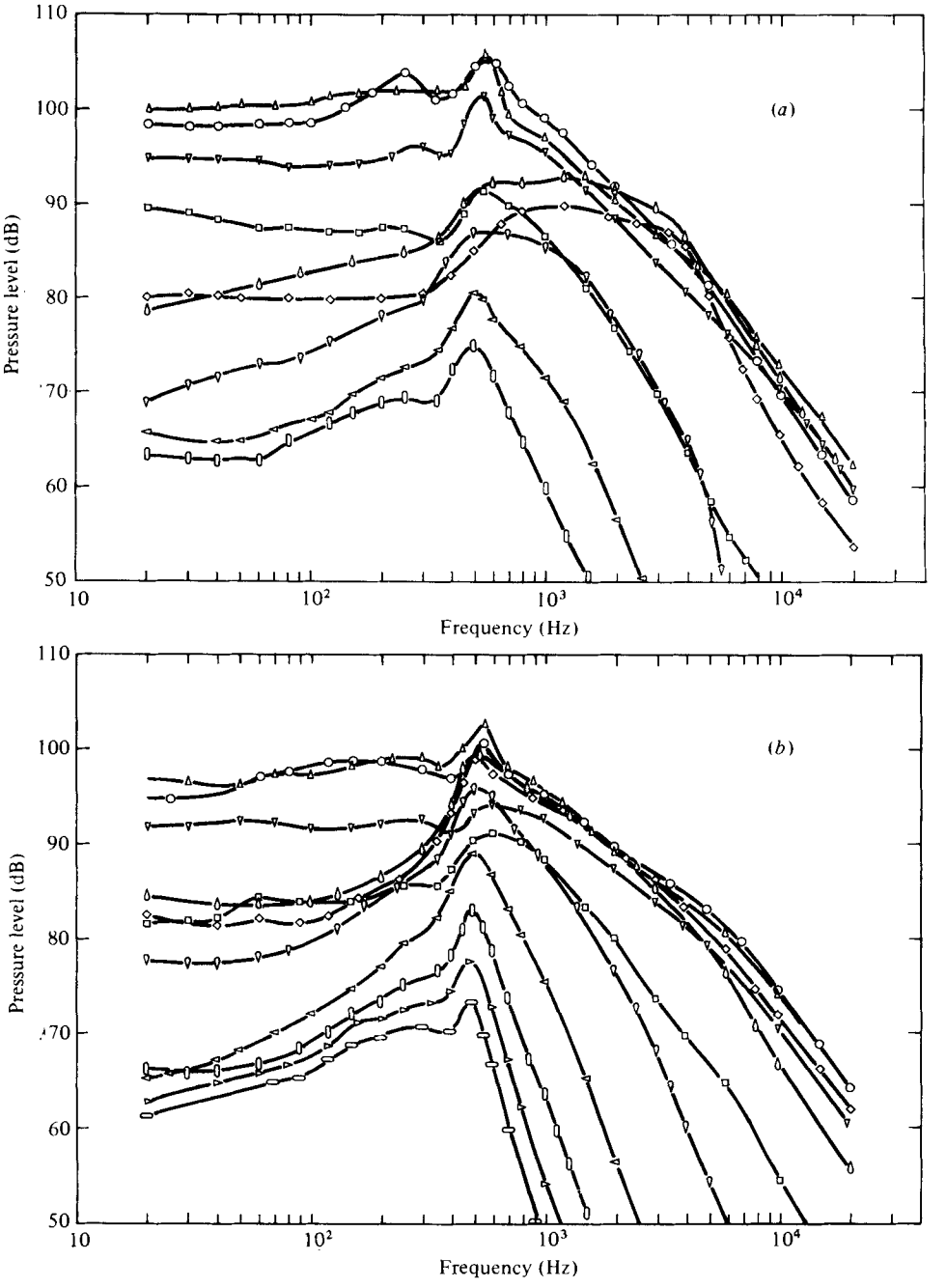

FIGURE 18. For legend see facing page.

radial position of about $y/D_o = 0{\cdot}15$. At $x/D_o = 0{\cdot}3$ and $x/D_o = 0{\cdot}4$ the maximum occurs at $y/D_o = 0{\cdot}15$ and at $y/D_o = 0{\cdot}1$ respectively. Besides the change in the position of the maximum, the level also changes, 100 dB at $x/D_o = 0{\cdot}2$, 107 dB at $x/D_o = 0{\cdot}3$ and 106 dB at $x/D_o = 0{\cdot}4$.

The pressure spectra immediately downstream of the internal recirculating region are shown in figures 18(*a*)–(*d*). In the region of $0{\cdot}5 \leqslant x/D_o \leqslant 1$ the more distinct peak

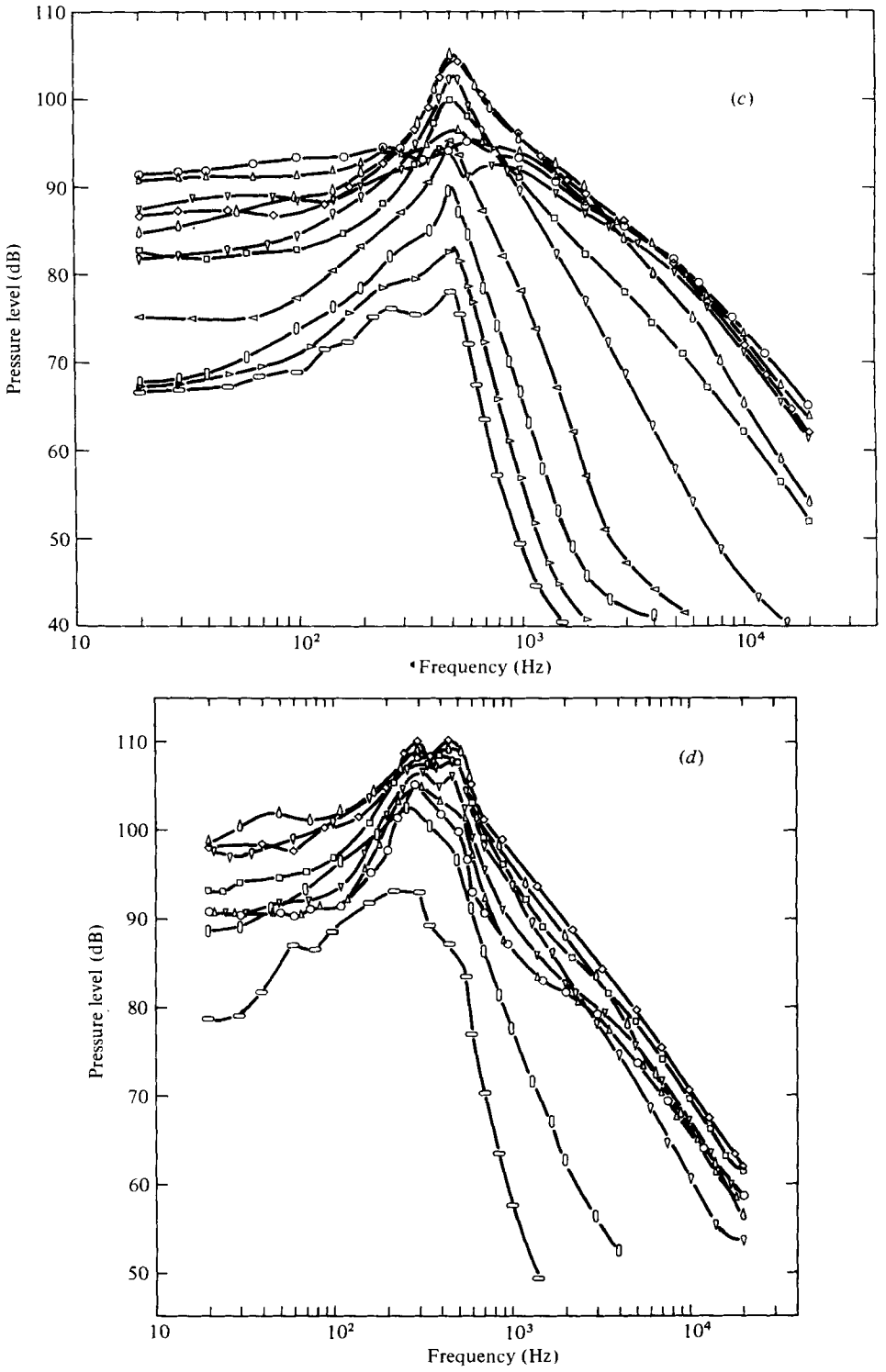

FIGURE 18. Spectra of pressure fluctuations within inner mixing region of basic annular jet: (*a*) $x/D_o = 0{\cdot}5$; (*b*) $x/D_o = 0{\cdot}75$; (*c*) $x/D_o = 1{\cdot}0$; (*d*) $x/D_o = 2{\cdot}5$. y/D_o: ◇, 0·4; ⬡, 0·5; ⬡, 0·6; ◁, 0·7; ⬡, 0·8; ▷, 0·9; ⬭, 1·0. Other symbols as in figure 17.

is also present, but is having slightly higher frequency 500–550 Hz. The maximum also varies, though less, with the position: at $x/D_o = 0{\cdot}5$ it occurs at $y/D_o \simeq 0{\cdot}1$; at $x/D_o = 0{\cdot}75$ it is at $y/D_o = 0{\cdot}1$ and $x/D_o = 1$ at $y/D_o = 0{\cdot}1$. The respective maximum level is 106, 103, and 105 dB.

This more distinct peak at 500 Hz is not only found in the inner region but also in some parts of the potential core and in the outer mixing region. This is clearly illustrated by the spectra obtained for the radial positions $y/D_o \geqslant 0{\cdot}3$ (figure 18*a–d*). Nevertheless, the peak is absent at the position of $x/D_o = 0{\cdot}5$, $y/D_o = 0{\cdot}4$, at $x/D_o = 0{\cdot}75$, $0{\cdot}2 \leqslant y/D_o \leqslant 0{\cdot}3$ and at $x/D_o = 1$, $y/D_o = 0{\cdot}2$.

At both the axial positions $x/D_o = 0{\cdot}75$ and 1 two maximum levels of this 500 Hz are found (figure 18*b*, *c*). At the former position one is found at $y/D_o = 0{\cdot}1$ with a level of 103 dB, while the other is at $y/D_o = 0{\cdot}5$, a level of 99·5 dB. At $x/D_o = 1$ one is at $y/D_o = 0{\cdot}1$, a level of 96 dB and the other at $y/D_o = 0{\cdot}5$, a level of 105 dB.

Even under the gradual dominance of the jet vortices (peak frequency of 250–300 Hz) in the outer mixing region (Chan & Ko 1978), this peak at 500 Hz can still be observed in the spectra obtained at $x/D_o = 2{\cdot}5$ (figure 18*d*). Furthermore, in comparison with the jet vortice it is still fairly dominant in the radial positions $0{\cdot}2 \leqslant y/D_o \leqslant 0{\cdot}6$. The maximum of the peak level occurs at $y/D_o = 0{\cdot}4$ with a level of 110 dB.

Based on the pressure spectra shown in figures 17 and 18, and others which are not presented in this paper, the pressure intensity $\tilde{p}/\rho_o \overline{U}_o^2$ due to this more distinct peak at about 500 Hz is obtained (figure 19). As in the case of the conical jet, it was estimated by considering the contribution of the peak around 500 Hz in comparison with the total contributions from other sources. It is extremely interesting to find two separate regions of high pressure intensity of this 500 Hz peak. One region, as would be expected, is located behind the interface at the nozzle exit and is mainly found within the first diameter D_o downstream. The extent in the radial direction is mainly within the inner region. The other region is found within the outer mixing region, the potential core, the downstream part of the inner region and part of the entrainment region outside the jet. The extent of this region covers a much bigger area than the one behind the interface.

A closer look at the high pressure intensity region behind the interface shows the build-up of the intensity within the internal recirculating region (figure 19). It reaches a maximum of 1·4% just outside the boundary of the internal recirculating region, $x/D_o \simeq 0{\cdot}5$ before it decreases to 0·4% at $x/D_o = 1{\cdot}0$. It also shows from the contours that the high pressure intensity region is mainly bounded by the 0·4% contour.

The locations of the maximum pressure intensity are also shown in figure 19. Inside the internal recirculating region the locus of the maximum intensity is found to be deflected towards the central axis. Outside the internal recirculating region it is more or less parallel to the central axis. The positions of the maximum and minimum mean static pressure are included in the figure. It is found that the minimum mean static pressure is located on the locus of the maximum pressure intensity.

Axial distribution of the maximum pressure intensity is shown in figure 20. Also included is the distribution of the maximum overall pressure intensity. The highest level of the maximum intensity of the 500 Hz peak is 1·4% compared with 3·4% overall. In other words, the contribution from the 500 Hz peak is not the only dominant one and the contributions from other sources are just as important.

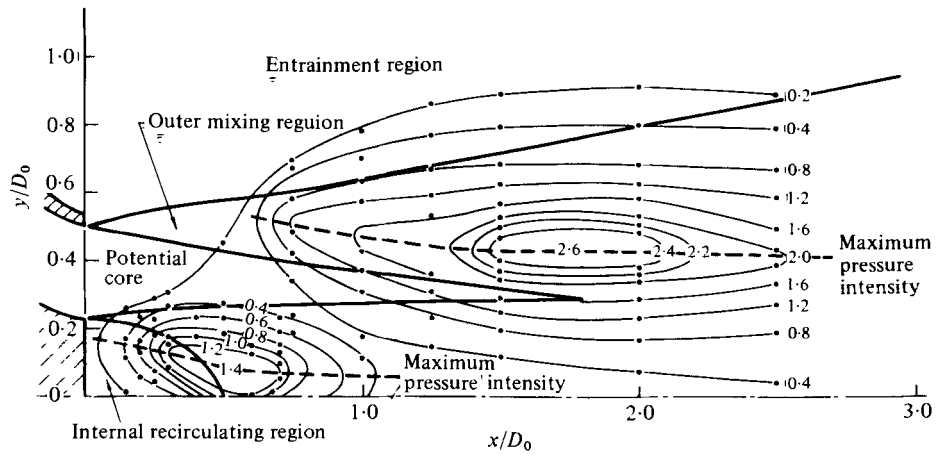

FIGURE 19. Pressure intensity contours caused by wake vortices within basic annular jet.

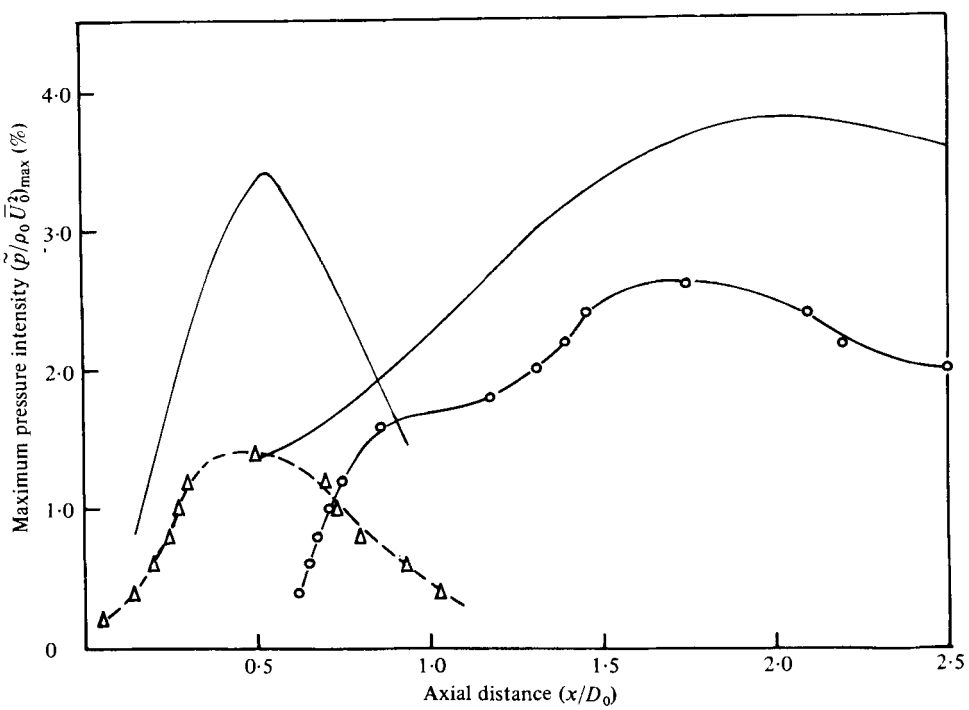

FIGURE 20. Axial distributions of the maximum pressure intensity due to wake vortices within basic annular jet. ——, overall; △, wake vortices; ○, induced by wake vortices.

From the results shown above it is obvious that the 500 Hz peak and its pressure intensity immediately behind the interface is due to the standing or wake vortices generated and their propagation downstream. The 0·4 % contour of the intensity indicates the boundary within which the effect of these wake vortices is felt. This means that the effect is felt not only in the internal recirculating region but also within the inner region up to the axial position of $x/D_o = 1{\cdot}0$.

The distribution of the pressure intensity suggests the rapid increase in the intensity

as the standing vortices start to propagate downstream. This rapid increase also suggests that the increase occurs mostly in the initial stage of their detachment, that is, within the internal recirculating region. This increase is associated with the sub-atmospheric region within the recirculating region (figure 7). The cause of the increase may partly be owing to the build-up of the wake vortices during their propagation downstream. It may also be due to the contribution from other shedding wake vortices.

The centre of the standing vortex and the location of the minimum mean static pressure, as obtained above (figures 4 and 7), lie on the locus of the maximum pressure intensity. This implies that the centre of the vortex is responsible for the minimum mean static pressure and the maximum pressure intensity at that particular cross-section. This further supports the findings of Ko & Davies (1975) and Ko & Kwan (1976) that the maximum pressure intensity, in overall terms, indicates the location of the vortices and their path of propagation downstream.

The propagation of the wake vortices downstream is affected by the entrainment behind the interface. The more rapid shifting of the vortices towards the central axis within the internal recirculating region may be owing to the fairly large sub-atmospheric region near the central axis (figure 7) and the reverse flow condition inside the recirculating region (figure 2). It may also be due to the alternate shedding of the standing vortex. Correspondingly, the above-atmospheric region immediately outside the internal recirculating region and the maximum mean static pressure lying at the central axis may be responsible for the more parallel path of the vortices in this region, but not along the axis.

The pressure intensity of the wake vortices builds up to its maximum within an axial distance of only 0·25–0·3 D_o from the vortex centre (figure 19). It takes another axial distance of 0·5 D_o for their disappearance. In other words, the vortices decay at $x/D_o \simeq 1{\cdot}0$. This axial position is also the limit where the mean static pressure becomes nearly atmospheric (figure 7). This implies that the wake vortices, which have as high a maximum pressure intensity as 1·4 % (the maximum overall pressure intensity in the outer mixing region is 3·8 %), disappear only within an axial distance of 0·75 D_o after their formation. This distance is really small in comparison with the one of the jet vortices found in the outer mixing region, about 5·0 D_o (Chan & Ko 1978).

The cause for this rapid disappearance of the wake vortices is not really known. It may be due to the cancellation of the different wake vortices shedding from different parts behind the interface, especially after they are shifted towards the central axis. However, the experimental investigation of vortex shedding from a bluff body within a uniform and a shear flow of Maull & Young (1973) could still detect very strong vortices after six base diameters downstream. This is much bigger than the axial distance of 2·2 D_i (or 1·0 D_o) where the wake vortices disappear in the present study. Care has to be taken for the comparison because the situation of Maull & Young (1973) is basically two-dimensional while the present one is axisymmetrical.

Some clues on the rapid decay or suppression may be indicated by the Strouhal number distribution of the wake vortices (table 1). The Strouhal numbers based on both the inner diameter D_i and outer diameter D_o are shown. It is interesting to find that within the inner region basically there are two Strouhal number groups, the first one being $0{\cdot}25 \leqslant St_i \leqslant 0{\cdot}26$ and the second $0{\cdot}30 \leqslant St_i \leqslant 0{\cdot}32$ (the corresponding peak frequencies are 450 Hz $\leqslant fw \leqslant$ 470 and 540 Hz $\leqslant fw \leqslant$ 570 Hz respectively).

y/D_o ... 0	0·05	0·1	0·15	0·2	0·25	0·3
x/D_o						
0·25 —	—	0·26	—	0·25	—	0·28
		(0·57)		(0·55)		(0·62)
0·3 —	0·25	0·26	0·26	0·25	0·28	0·28
	(0·55)	(0·57)	(0·57)	(0·55)	(0·62)	(0·62)
0·4 —	0·30	0·25	0·26	0·26	0·28	—
	(0·66)	(0·55)	(0·57)	(0·57)	(0·62)	
0·5 0·32	—	0·30	—	0·31	—	0·31
(0·71)		(0·66)	—	(0·68)		(0·68)
0·75 0·31	—	0·31	—	—	—	—
(0·68)		(0·68)				
1·0 0·31	—	0·31	—	—	—	—
(0·68)		(0·68)	—	—	—	—

† $St_i = f_w D_i/\overline{U}_o$; $St_o = f_w D_o/\overline{U}_o$.

TABLE 1. Strouhal number St_i (St_o)† produced by wake vortices in the inner region of basic annular jet.

The Strouhal number of the wake vortices is comparable with that of the vortex shedded from a two-dimensional bluff body of Maull & Young (1973). For uniform flow Maull & Young found the Strouhal number varied only slightly, $0{\cdot}24 \leqslant St \leqslant 0{\cdot}25$; for shear flow there was a jump in shedding frequency along the span of the body. If the Strouhal number was based on the centre-line velocity, a value of 0·21–0·31 was found. However, if it was based on the local velocity, a value of 0·25–0·27 was found. Thus, it can be seen from table 1 that the Strouhal numbers obtained behind the interface agree well with the ones of Maull & Young (1973) though the conditions are different. It further supports the proposed model that wake vortices are shedded behind the interface at the nozzle exit.

A more detailed look at the distribution of the two groups of Strouhal number indicates that the first group of $0{\cdot}25 \leqslant St_i \leqslant 0{\cdot}26$ is mainly found inside the internal recirculating region (table 1). The jump in the peak frequency or Strouhal number to the value of the second group, $0{\cdot}30 \leqslant St_i \leqslant 0{\cdot}32$, occurs in the inner mixing region, $x/D_o \geqslant 0{\cdot}5$. This distinction in the region of these two groups of the Strouhal number is interesting. This means that in the region where the flow velocity is low and reversed (figure 2), that is, in the internal recirculating region, the peak frequency or Strouhal number is slightly lower. The near constancy in the whole recirculating region suggests that it behaves like a cell (Gaster 1971; Maull & Young 1973). In actual fact, Gaster (1971) and Maull & Young (1973) used the term cell to represent the span of the two-dimensional body where the frequency of vortex shedding was constant. It is slightly different from the meaning above in that it only represents the region having constant peak frequency of the standing vortices as they propagate downstream. However, the constant frequency behaviour like a cell occurs within the internal recirculating region where the shear flow can vary to as high as 0·3–0·4 of the jet exit velocity (figure 2).

The jump in the peak frequency or Strouhal number from 450–470 to 540–570 Hz occurs when the wake vortices propagate into the inner mixing region where the local mean velocity is higher and in the same direction downstream. In this region the shear flow can vary even higher, to as high as 0·6–0·7 of the jet exit velocity (figure 2).

This jump in the peak frequency of the wake vortices in this cell may be partly owing to the higher mean velocity experienced by the wake vortices. However, since the change in the mean velocity is fairly gradual, it does not explain why the jump occurs. Nevertheless, the jump of this study may be analogous to the shear flow condition of Gaster (1971) and Maull & Young (1973) that, the higher the local velocity, the higher the frequency of the vortex shedded.

The smoke photographs of the flow of Maull & Young (1973) indicated that the divisions between the cells along the span of the body were marked with longitudinal vortices lying in the free-stream direction. With the addition of a strong longitudinal vortex the above authors have found a significant change in the shedding frequency. In a similar study Kuethe (1972) introduced longitudinal vorticity into the wake of airfoil by placing vortex generators at the trailing edge and found that the vortex shedding is suppressed. It thus seems from the observations of the above workers that the presence of introduced longitudinal vortices would suppress the vortex shedded and render a more significant jump in the peak frequency across the cells.

Although the flow situations of the above workers are different from those of the present study it seems that a similar phenomenon is being found in the present case of the wake vortices shedded behind the interface. The suppressed vortices and the jump in peak frequency, as shown in figure 19 and table 1, agree with the above phenomenon. But in the present case the responsible longitudinal vortices have still to be found. As will be discussed in the later section, the responsible vortices may be caused by another train of jet vortices generated in the inner mixing region. These jet vortices are generated owing to the shear of the mean flow in the potential core with the flow in the internal recirculating region. The evidence of these jet vortices has been shown by the very small peak at $x/D_o = 0{\cdot}4$ and $y/D_o \simeq 0{\cdot}2$ in the overall pressure intensity contours (figure 12). Furthermore, it is immediately downstream of the peak that the jump in the peak frequency is found ($x/D_o = 0{\cdot}5$). This furnishes some support for the influence of the inner jet vortices on the behaviour of the wake vortices inside.

The above discussion suggests the probable cause for the behaviour of the wake vortices found behind the interface of the basic annular jet. Further research would still have to be done to find the exact causes and mechanism involved. Even in the basically two-dimensional cases of Gaster (1971), Kuethe (1972) and Maull & Young (1973) the mechanism of the formation of the cells and the parameters governing them are still not known; or is there good knowledge of the effect of axisymmetry on the mechanism affecting the wake vortices or on the cells, which are not aligned as the two-dimensional cases. It is also not known how the inner jet vortices, not really having very high intensity, would trigger, if the hypothesis is right, the jump in frequency and the suppression of the wake vortices. In addition, it is not yet known what the relationship is of the Strouhal number of the inner jet vortices with that of the wake vortices.

The other very interesting phenomenon shown by the pressure intensity contours in figure 19 is the big pressure intensity region in the outer mixing region of the basic annular jet. As in the case of the wake vortices discussed above, the pressure intensity is mainly caused by the contributions around 500 Hz. As has been discussed by Chan & Ko (1978), for the conical and ellipsoidal jet, which has the bullet introduced behind the interface, the peak in the pressure spectrum is due to the jet vortices

y/D_o ... 0	0·1	0·2	0·3	0·4	0·5	0·6	0·7	0·8	0·9	1·0
x/D_o										
1 —	—	0·65	0·62	0·65	0·62	0·62	0·62	0·65	0·62	0·62
		(0·29)	(0·28)	(0·29)	(0·28)	(0·28)	(0·28)	(0·29)	(0·28)	(0·28)
1·25 —	0·60	0·62	0·65	0·65	0·65	0·62	0·62	0·62	0·62	0·60
	(0·27)	(0·28)	(0·29)	(0·29)	(0·29)	(0·28)	(0·28)	(0·28)	(0·28)	(0·27)
1·5 —	0·62	0·62	0·62)	0·62	0·65	0·65	0·62	0·65	0·62	—
	(0·28)	(0·28)	(0·28)	(0·28)	(0·29)	(0·29)	(0·28)	(0·29)	(0·28)	—
1·75 —	0·62	0·65	0·62	0·65	0·62	0·60	0·62	0·62	0·62	0·60
	(0·28)	(0·29)	(0·28)	(0·29)	(0·28)	(0·27)	(0·28)	(0·28)	(0·28)	(0·27)
2 0·62	0·65	0·65	0·65	0·65	0·62	0·65	0·60	0·60	0·60	0·60
(0·28)	(0·29)	(0·29)	(0·29)	(0·29)	(0·28)	(0·29)	(0·27)	(0·27)	(0·27)	(0·27)
2·25 0·62	0·62	0·65	0·60	0·62	0·60	—	—	—	—	—
(0·28)	(0·28)	(0·29)	(0·27)	(0·28)	(0·27)					
2·5 0·60	0·62	0·58	0·58	0·58	0·60	0·60	0·58	0·58	0·58	0·58
(0·27)	(0·28)	(0·26)	(0·26)	(0·26)	(0·27)	(0·27)	(0·26)	(0·26)	(0·26)	(0·26)

† $St_o = f_w D_o/\bar{U}_o$; $St_i = f_w D_i/\bar{U}_o$.

TABLE 2. Strouhal number St_o (St_i)† induced by wake vortices of basic annular jet.

generated in the outer mixing region (figures 13 and 14). In other words the 500 Hz peak, as found in the basic annular jet, is absent. Thus the 500 Hz peak is limited to the basic annular jet and seems to be associated with the presence of the wake vortices behind the interface.

The high pressure intensity region covers not only the outer mixing region but also a certain part of the potential core and the inner region (figure 19). This area is much bigger than that of the wake vortices. From the axial distance of $x/D_o = 0{\cdot}6$ maximum pressure intensity is observed at each section, though it is always found within the outer mixing region. The axial distribution of the maximum pressure intensity is shown in figure 20, in which the overall intensity is also shown. The intensity of the 500 Hz peak is 2·6 % and is slightly lower than that overall, 3·8 %. This difference is mainly due to the contributions from the jet vortices in the outer mixing region.

The axial position of the peak maximum pressure intensity of the 500 Hz peak is located at $x/D_o = 1{\cdot}75$ (figures 18 and 19) and is slightly further upstream than the peak of the overall intensity, $x/D_o = 2$. If the jet vortices only are considered, their peak location is found at $x/D_o = 3{\cdot}5$ (figure 10) and is about 1·75 D_o further downstream than the peak intensity at 500 Hz. In this respect, it can be easily visualized that the overall peak is due to the combination of the effects from both peaks of the spectrum. The locus of the maximum pressure intensity of the 500 Hz peak, as indicated in figure 19, has the same trend as that for the jet vortices (figure 10). However, it is slightly further away from the central axis.

The distribution of the Strouhal number of this 500 Hz peak is tabulated in table 2. The Strouhal numbers, St_o and St_i, based on the outer and inner diameter, are shown. Except for the position of $x/D_o = 2{\cdot}5$, the Strouhal numbers obtained at other positions shown in the table are nearly constant, $0{\cdot}60 \leqslant St_o \leqslant 0{\cdot}65$ ($0{\cdot}27 \leqslant St_i \leqslant 0{\cdot}29$). The Strouhal numbers at $x/D_o = 2{\cdot}5$ are slightly lower, $0{\cdot}58 \leqslant St_o \leqslant 0{\cdot}62$ ($0{\cdot}26 \leqslant St_i \leqslant 0{\cdot}8$). This slight variation may be partly owing to the difficulty in determining the peak frequency from the spectral record.

The Strouhal numbers St_i in the outer mixing region agree well with the ones of the wake vortices behind the interface (table 1). However, their values are roughly between the ones of the wake vortices within the internal recirculating region and the ones within the inner mixing region downstream where the jump in the peak frequency or Strouhal number is observed. In addition, the near constaney of the Strouhal number within the outer mixing region investigated indicates that there is no jump in the peak frequency. This means that the whole outer mixing region has an excitation at the same peak frequency. This phenomenon is quite different from the behaviour of the jet vortices in the same region where an appreciable variation in the Strouhal number is found. (Ko & Davies 1971; Chan & Ko 1978). This further confirms that this big pressure intensity region is not caused by the jet vortices but is associated with the wake vortices inside the inner region of the basic annular jet.

The absence of any direct link in the pressure intensity contours in the outer mixing region with the inner region does not suggest direct propagation of the wake vortices into the outer region. Furthermore, it is not really possible for the wake vortices to propagate from the inner region of low mean velocity across the high mean velocity potential core into the outer mixing region. Thus, the most probable cause may be the propagation of disturbances of the wake vortices into the outer mixing region, resulting in the excitation of this outer shear layer.

Forcing of a single jet has been investigated by Crow & Champagne (1971), Chan (1974), Lee & Payne (1977), Moore (1977) and many others. The source of forcing was introduced either upstream of the nozzle exit (that is, in the plenum chamber) or just outside the nozzle exit. It has been found that the periodic surging at a particular frequency and amplitude at the jet exit resulted in the development of a distinct wave system. The wavelength was a function of the forcing frequency and the jet velocity. The amplitude of the wave reached a maximum and then gradually decayed downstream. Whether the mode was preferred or not depended on the Strouhal number based on frequency, exit velocity and diameter. The Strouhal numbers of the most preferred mode was around 0·60 and depended on the location of the jet, either at the central axis or at the shear layer. The results of an acoustically forced single jet of Chan (1974) have shown that the location of the peak of the pressure distribution of the disturbances in the shear layer seemed to be independent of Strouhal number. It took a value of $(x/D)\,St = 0{\cdot}94$. The Strouhal number range covered was from 0·3 to 0·8.

The Strouhal number St_o, based on the outer diameter D_o, of the wake vortices behind the interface of the present investigation varies from 0·55 to 0·62 in the internal recirculating region and from 0·66 to 0·71 in the inner mixing region behind it (table 1). These Strouhal numbers are the same as that of the most preferred mode found for the single jet. This means that the disturbances of the wake vortices would very easily excite the jet, that is, the shear layer at its most preferred mode of excitation. This is borne out by the near constant Strouhal number St_o of 0·58–0·62 in the outer mixing region of the basic annular jet (table 2). By using the value of $(x/D)\,St = 0{\cdot}94$ of Chan (1974), the location of the peak of the pressure distributions in the outer mixing region or shear layer of the present annular jet is estimated at $1{\cdot}5 \leqslant x/D_o \leqslant 1{\cdot}6$. This agrees very well with the actual location of the peak at $x/D_o \simeq 1{\cdot}75$ found in figures 18 and 19.

Although agreement of the location of the peak in these two cases is good, differences

have been found. For the case of Chan (1974) the forcing acoustic disturbance was generated upstream of the nozzle exit. An amplitude was set at 125 dB [corresponding to a fluctuating (r.m.s.) velocity ratio $\tilde{u}_e/\overline{U}_o = 0{\cdot}13\,\%$ for an assumed plane wave] at the centre of the nozzle exit with the jet running. Under these conditions there was an amplification of about 18 dB (an amplification coefficient of 7·9) at the centre of the shear layer. In the present case, however, the disturbance is mainly due to the wake vortices generated inside the internal recirculating region and their propagation downstream. The maximum spectral level is only 106 dB (corresponds to $\tilde{u}_e/\overline{U}_o = 0{\cdot}02\%$) and is located at the position of $x/D_o = 0{\cdot}5$ and $y/D_o \simeq 0{\cdot}1$ (figure 18*a*). The similar amplification of the spectral peak above the background level in the outer mixing region is only about 5 dB (an amplification coefficient of 1·8). This is much lower than the amplification of the single jet of Chan (1974). Nevertheless this lower amplification is expected. It is because, as Crow & Champagne (1971) have found, the response at the centre-line of single jet increases with the increase in the forcing amplitude. The amplification depends on the forcing amplitude whether it is above or below the saturation point where linearity is observed. A rough estimate of the amplification of the preferred mode at the centre-line of Crow & Champagne (1971) at the same tiny forcing level of 0·02 % as the present investigation gives a value of 1·4. It is of the same order of magnitude as the amplification of 1·8 in the present study.

Although agreement of the results obtained in the outer mixing region of the basic annular jet with the results of a forced single jet is good, suggesting excitation of the outer shear layer by the disturbances of the wake vortices, questions on the basic mechanism have still to be answered before better understanding can be achieved. It is not really known why the disturbances can excite the outer mixing region but neither the inner shear layer nor the centre of the jet. Part of the explanation may be that the Strouhal number of the wake vortices is different from that of the most preferred mode of the inner region. Even if there is any excitation or wave set-up, would the inner jet vortices present suppress or inhibit it? The findings in the outer mixing region seems to suggest that if the Strouhal numbers are at or near that of the most preferred mode, they tend not to interfere with each other. Nevertheless, one is apt to wonder how or why the two waves, owing to the outer jet vortices and to the wake vortices, which are fairly close in the peak frequency, can still be so distinct in their characters in the whole of the outer mixing region.

Though the above discussion on the forcing level caused by the wake vortices was based on the peak spectral level, one does not know how the excitation at other frequencies around the peak affects the forcing of the outer mixing region. Nor does one know how these disturbances propagate through the high mean velocity region of the potential core. In other words, where and how do the disturbances act such that the wave in the outer mixing region is formed? Do the disturbances excite the unstable region at or very near the nozzle exit? The contours of the pressure intensity in figure 19 show the region where the 500 Hz peak is observed. This means that within the part of potential core and of the outer mixing region just outside the nozzle exit no 500 Hz peak is found. This implies either that the disturbance is absent or that the level is too low to be picked up by the microphone or masked by the tiny background level. If the hypothesis of absence of disturbance is right, the disturbance might only excite the outer shear layer at a location where the amplification rate is not high (Chan 1974).

Looking again at the spectra shown in figure 17, another broader peak is also found at the radial position of $0{\cdot}2 \leqslant y/D_o \leqslant 0{\cdot}3$. The peak frequency of this broad peak, though slightly more difficult to determine, centres around 1–1·2 kHz. At the axial position of $x/D_o = 0{\cdot}2$ the peak seems to be located at $y/D_o = 0{\cdot}25$ and for $x/D_o = 0{\cdot}3$ at $y/D_o \simeq 0{\cdot}25$ (figure 17*a*, *b*). For the axial positions of $x/D_o = 0{\cdot}4$ and 0·5, the peak is nearly absent from the spectrum (figure 17*c*, *d*). Reappearance of the broad peak occurs at the position of $x/D_o = 0{\cdot}75$, $y/D_o = 0{\cdot}2$ and $x/D_o = 1{\cdot}0$, $y/D_o = 0{\cdot}1$ (figure 18*b*, *c*). At these two positions the peak frequency is lower (about 800 Hz). Comparison with the results for a single jet of Ko & Davies (1971) has found that the spectral shape of the broad peak is fairly similar to that in their experiments very near the nozzle exit.

The disappearance of the broad peak at $0{\cdot}4 \leqslant x/D_o \leqslant 0{\cdot}5$ may be due to the masking by the high level of the wake vortices. As has been shown in figure 17(*a*), the broad peak has only a peak pressure level of about 88 dB. At these positions of

$$0{\cdot}4 \leqslant x/D_o \leqslant 0{\cdot}5$$

the wake vortices attain their maximum level. Even though the peak frequency is different, the level at other frequency of the wake vortices may still be sufficient to mask the tiny peak level of the broad peak.

The estimated locations of the maximum pressure intensity of this broad peak are also shown in figure 12. They lie in the inner mixing region between the potential core and the internal recirculating region. Near the nozzle exit it lies nearer to the boundary of the potential core and further downstream it shifts more towards the central axis. The wide scatter of the locations of the maximum pressure intensity is because of the difficulty in the determination of the exact location. The locus of this broad peak is very similar to those of the jet vortices in the outer mixing region (figures 10 and 11).

The distribution of the peak frequency of this broad peak in the inner mixing region is shown in figure 21. The maximum Strouhal numbers $(St_o)_{\max} = (f_j D_o/\overline{U}_o)_{\max}$ based on the outer diameter D_o, obtained in the inner mixing region are compared with the ones of the single jet of Ko & Davies (1971). With the exception of the result at $x/D = 0{\cdot}75$ of the single jet, the other data points seem to form a single straight line, irrespective of the annular or single jet. But the maximum Strouhal number at this axial position of $x/D = 0{\cdot}75$ for the single jet is the same as the Strouhal number at $x/D_o = 0{\cdot}2$ for the basic annular jet.

From the results presented above it seems highly likely that this broad peak inside the inner mixing region is caused by another train of jet vortices that is generated and its propagation downstream. The agreement of the small overall pressure intensity region found in figure 12 with the peak intensity distribution obtained from the spectrum suggests that the pressure region is caused by the jet vortices. The location of the maximum is at $x/D_o = 0{\cdot}4$ and $y/D_o = 0{\cdot}2$. The maximum overall intensity is only 1·8% instead of 3·4% for the wake vortices and 3·8% in the outer mixing region. However, it is comparable with the jet vortices in the outer mixing region of the conical jet, which is about 2·0% (figure 10). Similarly, the spectral peak level of 88 dB for the inner jet vortices is only slightly lower than the level of outer jet vortices in the outer mixing region, though they are located further downstream.

These inner jet vortices are found at least $0{\cdot}25\ D_o$ further upstream than the outer

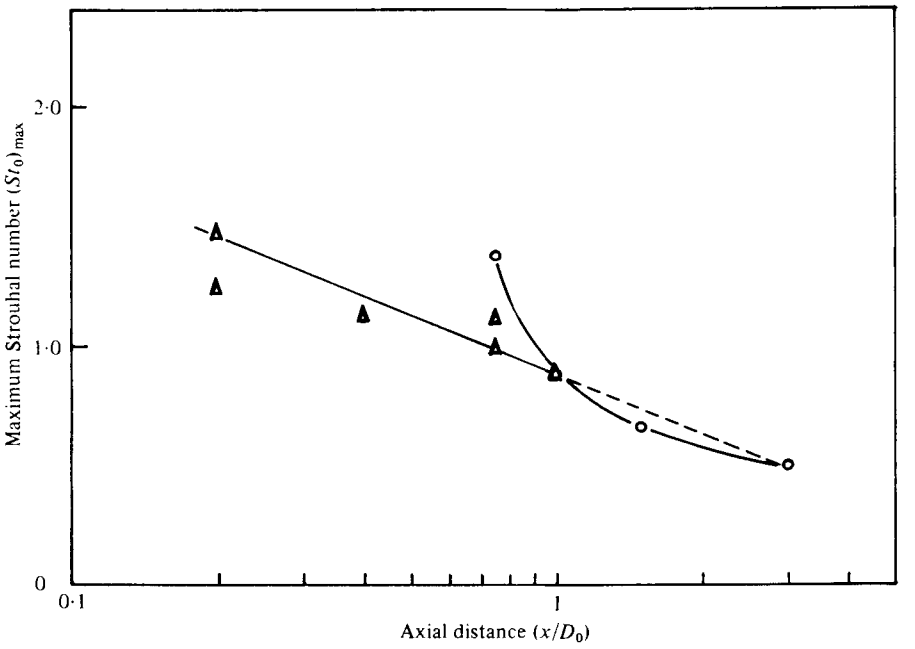

FIGURE 21. Axial distribution of the maximum Strouhal number of jet vortices inside inner mixing region of basic annular jet. △, basic annular jet; ○, single jet (Ko & Davies 1971).

ones. This earlier generation and building-up of the inner jet vortices may be due to the additional entrainment behind the interface and the internal recirculating region formed. The disturbances in the internal recirculating region may cause earlier development of the instability wave at the nozzle exit, resulting in the earlier formation of the inner jet vortices. The earlier development is supported by the agreement of the Strouhal number results for the basic annular and single jet. The data points of the single jet, except the one at $x/D = 0{\cdot}75$, fall very nicely on the extrapolated part of the straight line of the inner jet vortices results of the basic annular jet. In addition, the Strouhal number at $x/D = 0{\cdot}75$ of the single jet ($St_{max} = 1{\cdot}4$) is the same as the one at $x/D_o = 0{\cdot}2$ of the basic annular jet [$(St_o)_{max} \simeq 1{\cdot}4$]. The phenomenon may mean that irrespective of the ambient condition at the nozzle exit the jet vortices would require a certain fixed distance for their generation and development. For the single jet the small disturbances inherited from upstream of the nozzle exit excite the formation of the jet vortices at only $x/D = 0{\cdot}75$ with the same maximum Strouhal number of 1·4. However, this late appearance of the vortices is accompanied by a rapid change of its Strouhal number characteristics within a very short distance, about $0{\cdot}25\ D$, to the normal state. In the basic annular jet the additional entrainment and the higher disturbances generated behind the interface are responsible for the earlier generation of the jet vortices. The earlier appearance of these vortices is found at $x/D_o = 0{\cdot}2$ and they have the same maximum Strouhal number $(St_o) \simeq 1{\cdot}4$. This means that the earlier appearance allows the vortices to follow their normal development.

Although the above discussion is mainly based on determinations of the maximum Strouhal number, it is encouraging that Schlieren photographs of Bradshaw, Ferriss

& Johnson (1964), Crow & Champagne (1971) and Moore (1977) seem to support the above reasonings. For the unforced single jet the Schlieren photographs of the above workers show the appearance of the vortices at $0{\cdot}5 \leqslant x/D \leqslant 1$, followed by fairly rapid change in the structure of the vortices. For the forced single jet the Schlieren photographs seem to suggest slightly earlier appearance of the vortices. The photographs of Moore (1977) at different drive levels indicate that the higher the drive level, the closer to the nozzle exit the vortices start to appear.

The inner jet vortices of the basic annular jet seem to disappear after the first outer diameter D_o downstream of the nozzle exit. The disappearance may be because the vortices, having the Strouhal number $0{\cdot}9 \leqslant (St_o)_{\max} \leqslant 1{\cdot}4$, are different from the most preferred mode. It is not known whether the wake vortices may suppress the jet vortices or not.

It was pointed out by Chan & Ko (1978) that, within the internal recirculating region and the region immediately downstream, the fairly broad peak at about 260 Hz is not due either to the outer nor the inner jet vortices. Additional information obtained in the present study has shown that this peak is mainly observed within the region where the wake vortices are found (figures 12 and 18). The peak of the maximum pressure intensity is located at $x/D_o = 0{\cdot}4$ and $y/D_o = 0{\cdot}08$, that is, within the internal recirculating region. This location is slightly further downstream and more towards the central axis than the location of the vortex centre, $x_c/D_o = 0{\cdot}22$ and $y_c/D_o = 0{\cdot}18$ (figure 5). Nevertheless, this location is further upstream than that of the wake vortices (figures 12 and 19). Thus even though the additional evidence is still not conclusive, it suggests that this 260 Hz peak may be due to the standing vortex.

The variation of the spectral shape of the pressure fluctuations inside the basic annular jet with exit velocity is shown in figure 22. The position of the microphone was $x/D_o = 2$ and $y/D_o = 0$. The range of exit velocity covered is $10 \leqslant \bar{U}_o \leqslant 60$ m s^{-1}. The above spectra can be compared with those of the conical jet (figure 23). The position of the microphone was $x/D_o = 2$ and $y/D_o = 0$. For both annular jets the jet and wake vortices are found at the velocity range covered, even though the jet vortices of the basic annular jet at 10 m s^{-1} are not so distinct. The corresponding Strouhal numbers of the jet vortices are $St_o = 0{\cdot}37$ for the basic annular jet and $St_o = 0{\cdot}23$ for the conical jet over the exit velocity $20 \leqslant \bar{U}_o \leqslant 60$ m s^{-1}. That associated with the wake vortices is $0{\cdot}28 \leqslant St_i \leqslant 0{\cdot}30$ for the basic annular jet and $2{\cdot}2 \leqslant St_i \leqslant 2{\cdot}7$ for the conical jet.

8. Conclusions

The complexity in the flow structure in annular jets depends greatly on the presence or absence of the bullet behind the interface at the nozzle exit. With the introduction of the bullet, as in the conical and ellipsoidal jet, the internal recirculating region is eliminated. In this respect, the flow structure of these annular jets is comparatively simple. In the outer mixing region similarity of the mean velocity and turbulence intensity profiles of these annular jets has been found. Further, they agree very well with the single jet. Also in the conical and ellipsoidal jet the flow structure is dominated by the presence of a train of jet vortices. These vortices have the same characteristics as those of the vortices observed in the single jet. In the inner region,

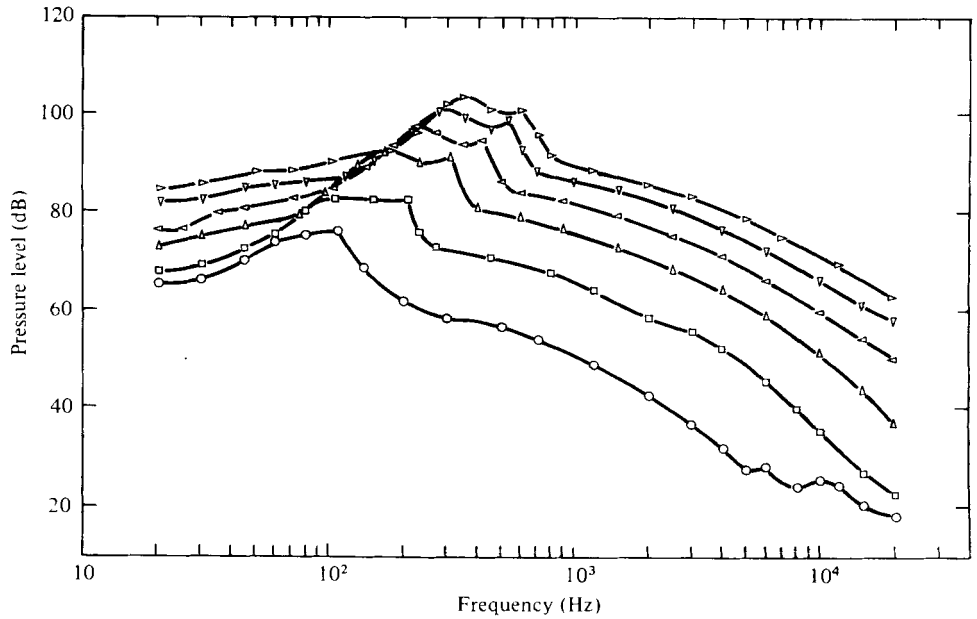

FIGURE 22. Spectra of pressure fluctuations at different jet exit velocities of basic annular jet. ($x/D_o = 2$, $y/D_o = 0$). $\bar{U}_o$(m s^{-1}): ○, 10; □, 20; △, 30; ◁, 40; ▽, 50; ▷, 60.

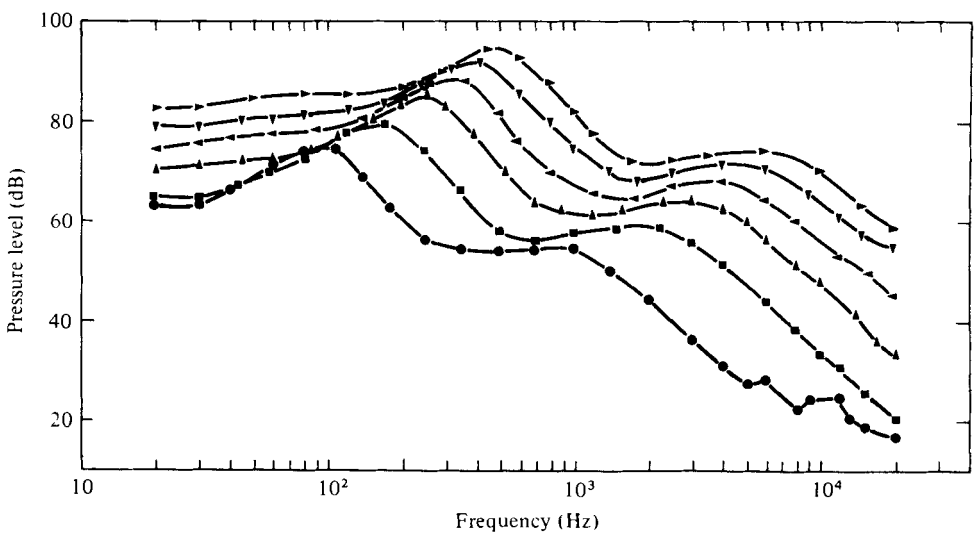

FIGURE 23. Spectra of pressure fluctuations at different jet exit velocities of conical jet. ($x/D_o = 2$, $y/D_o = 0$). $\bar{U}_o$(m s^{-1}): ●, 10; ■, 20; ▲, 30; ◀, 40; ▼, 50; ▶, 60.

however, even though the introduction of the bullet eliminates the internal recirculating region and its vortices, wake vortices have been formed in the boundary layer on the surface of the bullet. These wake vortices separate and propagate downstream and their effect can still be felt up to four outer diameters D_o downstream and mainly along the central axis ($y/D_o \leqslant 0{\cdot}1$). The peak frequency or Strouhal number of these wake vortices varies with respect to the shape of the bullet, conical

or ellipsoidal. Immediately downstream of the tip of the bullet, the Strouhal number of the wake vortices of the conical jet is higher than the one of the ellipsoidal jet. Further downstream, they become the same.

In the basic annular jet the bullet is absent, resulting in the formation of the internal recirculating region and the inner mixing region, that is, the inner region. It is perhaps because of the shrouding effect of the annular potential core that the main properties of the outer mixing region of the basic annular jet are basically the same as those of the conical, ellipsoidal and single jet. In other words, similarity in the mean velocity and turbulence intensity profiles and the presence of the train of jet vortices are found.

In the inner region of the basic annular jet, although reverse flow is found in the internal recirculating region, similarity in the mean velocity profiles in part of the region is found. But it has not been possible to find similarity in the region behind it. Further, the results from detailed mean static pressure measurements suggest the non-dimensional parameter of $M_o/A_i P_{\text{atm}}$ which represents the available pressure for the entrainment behind the interface. It is interesting to find that the vortex centre, the location of reattachment, the minimum and maximum mean static pressure and their locations correlate very well with the non-dimensional pressure. The good correlation with these mean parameters suggests the important relationship of the available pressure $M_o/A_i P_{\text{atm}}$ in the entrainment with the flow structures in the inner region.

The fluctuating pressure measurements in the inner region of the basic annular jet show a very complicated picture of flow structure. Within the internal recirculating region and the region behind it the flow is dominated by the standing vortices and their propagation downstream. But the region, where the effect of these wake vortices is felt, covers only the internal recirculating region and the inner region up to $x/D_o = 1$. Instead of the large distance downstream, where for instance the von Kármán vortex street is still felt, the small area of the wake vortices suggests suppression of these vortices. The suppression, accompanied by a jump in the Strouhal number, may be due to the presence of another train of vortices in the inner region of the basic annular jet.

The other train of vortices in the inner region is generated in the inner mixing region or shear layer where the shear between the potential core and the internal recirculating region occurs. These inner jet vortices, being generated further upstream than those of the outer mixing region, build up their intensity and decay fairly quickly, again within a distance of about one outer diameter D_o from the nozzle exit. The earlier generation of the inner jet vortices may be due to the presence of the internal recirculating region and the extra disturbances due to the wake vortices. These extra disturbances may affect the instability wave in the inner mixing region, resulting in the earlier formation of the inner jet vortices. The fairly rapid decay of the inner jet vortices may be because they are not at the most preferred mode. It may also be due to the disturbances of the wake vortices having Strouhal number different from the most preferred one in the inner mixing region.

The outer mixing region of the basic annular jet seems to be excited by the disturbances of the wake vortices propagating across the potential core. The excitation either in the form of a wave or another train of vortices occurs within the whole of the outer shear layer and within the adjacent regions. This fairly severe excitation may

be due to the disturbances of the wake vortices having the same Strouhal number as the most preferred mode of the outer mixing region. In this respect, even the very small level of disturbance may be able to excite the whole outer shear layer. The presence of this excitation implies that the outer mixing region is under two trains of vortices or waves, the outer jet vortices and the one associated with the wake vortices. It is only through their slightly different Strouhal number characteristics that they could be isolated in the present study.

REFERENCES

ABRAMOVICH, N. 1963 *The Theory of Turbulent Jets*. M.I.T. Press.

AYUKAWA, K. & SHAKOUCHI, T. 1976 Analysis of a jet attaching to an offset parallel plate. *Bull. Japan Soc. Mech. Engrs* **19**, 395–401.

BARRETT, R. V. & TIPPING, J. C. 1962 An investigation into the effects of ground proximity on twin coaxial annular jets, using hot and cold air. *Aero. Res. Counc. C.P.* no. 578.

BECHERT, D. W. & PFIZENMAIER, E. 1977 Amplification of jet noise by a higher-mode acoustical excitation. *A.I.A.A. J.* **15**, 1268–1271.

BEER, J. M. & CHIGIER, N. A. 1972 *Combustion Aerodynamics*. London: Applied Science Publishers Ltd.

BRADSHAW, P., FERRISS, D. M. & JOHNSON, R. F. 1964 Turbulence in the noise producing region of a circular jet. *J. Fluid Mech.* **19**, 591–624.

BRYER, D. W. & PANKHURST, R. C. 1971 *Pressure Probe Methods for Determining Wind Speed and Flow Direction*. H.M.S.O.

CARMODY, T. 1964 Establishment of the wake behind a disc. *Trans. A.S.M.E., J. Basic Engng* D **86**, 869–882.

CHAN, W. T. & KO, N. W. M. 1978 Coherent structures in the outer mixing region of annular jet. *J. Fluid Mech.* **89**, 515–533.

CHAN, Y. Y. 1974 Spatial waves in turbulent jets. *Phys. Fluids* **17**, 46–53.

CHIGIER, N. A. & BEER, J. M. 1964 The flow region near the nozzle in double concentric jets. *Trans. A.S.M.E., J. Basic Engng* D **86**, 797–804.

CROW, S. C. & CHAMPAGNE, F. H. 1971 Orderly structure in jet turbulence. *J. Fluid Mech.* **48**, 547–591.

DAVIES, P. O. A. L., FISHER, M. J. & BARRETT, M. J. 1963 The characteristics of the turbulence in the mixing region of a round jet. *J. Fluid Mech.* **15**, 337–367.

DAVIES, T. W. & BEER, J. M. 1969 The turbulence characteristics of annular wake flow. Heat and Mass Transfer in Flows with Separated Regions. *Int. Sem., Hercig-Novi, Yugoslavia.*

DURÃO, D. F. G. & WHITELAW, J. H. 1978 Velocity characteristics of the flow in the near wake of a disk. *J. Fluid Mech.* **85**, 369–385.

GASTER, M. 1971 Vortex shedding from circular cylinders at low Reynolds numbers. *J. Fluid Mech.* **46**, 749–756.

KO, N. W. M. & CHAN, W. T. 1978 Similarity in the initial region of annular jets: three configurations. *J. Fluid Mech.* **84**, 641–656.

KO, N. W. M. & DAVIES, P. O. A. L. 1971 The near field within the potential core of subsonic cold jets. *J. Fluid Mech.* **50**, 49–78.

KO, N. W. M. & DAVIES, P. O. A. L. 1975 Some covariance measurements in a subsonic jet. *J. Sound Vib.* **41**, 347–358.

KO, N. W. M. & KWAN, A. S. H. 1976 The initial region of subsonic coaxial jets. *J. Fluid Mech.* **73**, 305–335.

KUETHE, A. M. 1972 Effect of streamwise vortices on wake properties associated with sound generation. *J. Aircraft* **9**, 715–719.

KWAN, A. S. H. & KO, N. W. M. 1976 Coherent structures in subsonic coaxial jets. *J. Sound Vib.* **48**, 203–219.

KWAN, A. S. H. & KO, N. W. M. 1977 Covariance measurements in subsonic coaxial jets. *J. Sound Vib.* **52**, 567–578.

LAURENCE, J. C. 1956 Intensity, scale and spectra of turbulence in the mixing region of a free subsonic jet. *N.A.C.A. Rep.* no. 1292.

LEE, B. H. K. & PAYNE, L. F. 1977 Pressure measurements of spatial instability waves in an acoustically forced jet. *Nat. Aero. Establishment, Canada* LTR-HA-29.

MAULL, D. J. & YOUNG, R. A. 1973 Vortex shedding from bluff bodies in a shear flow. *J. Fluid Mech.* **60**, 401–409.

MILLER, D. R. & COMINGS, E. W. 1957 Static pressure distribution in the free turbulent jet. *J. Fluid Mech.* **3**, 1–16.

MILLER, D. R. & COMINGS, E. W. 1960 Force-momentum fields in a dual-jet flow. *J. Fluid Mech.* **7**, 247–256.

MOORE, C. J. 1977 The role of shear-layer instability waves in jet exhaust noise. *J. Fluid Mech.* **80**, 321–367.

SULLEREY, R. K., GUPTA, A. K. & MOORTHY, C. S. 1975 Similarity in the turbulent near wake of bluff bodies. *A.I.A.A. J.* **13**, 1425–1429.

TANAKA, T. & TANAKA, E. 1978 Experimental studies of a radial turbulent jet. *Bull. Japan Soc. Mech. Engrs* **21**, 665–672.